

The study describes the measurement of ice particle residual composition using the ALABAMA single particle mass spectrometer behind two specialized ice-selective inlets at the JFJ mountaintop station. Results are presented for several mixed phase cloud events and analyzed in the context of air mass history and previous JFJ IPR studies. This study adds what is still a fairly small list of ambient IPR studies and can potentially provide important information on glaciation for mixed-phase clouds over continental regions. However, the manuscript has numerous problems with data analysis and interpretation. This study might be saved by major revisions and what essentially amounts to a reanalysis of the dataset.

The results are very difficult to interpret and therefore have limited scientific impact. The difficulties result from a combination factors: 1) The compositional categories are muddled. 2) There are several artifact sources that omit important compositional markers, including Al and Si, unless further analysis can better differentiate the artifacts from real IPR. 3) The dataset is inherently small. Although this is to similar to other mountaintop IPR studies, it leads to a variety of inconsistencies in the dataset, particularly when comparing results from the two ice-selective IPR inlets and EM in Worrigen. 4) The study lacks other field measurements, even simple gas-phase tracers such as CO, to help decipher air mass histories and interpret the aerosol data instead relies completely on back-trajectory analysis.

Removing all suspect and speculative results would render this study too inconclusive to afford publication. This study hints at some interesting results, but often the authors present them without context or adequate description.

Changes in the manuscript are highlighted as follows:

Referee#1 → *yellow*
Referee#2 → *green*
Referee#3 → *red*
Additional changes → *blue*

Major comments

1) Inlet contamination

What is essentially a companion paper, (Worrigen) describes EM analysis of IPR, some of which were sampled at similar conditions, and is currently under review in ACPD. One principal finding from that study is that artifacts were generated from the ice crystal inlets used in the current study, with contamination rates sometimes being very large. Possible artifacts were addressed by the authors here and primarily include particles with Al, Si, and Pb. However, the artifacts analysis is based more on possibilities and suspicions than a demonstrated ability of ALABAMA to differentiate artifacts. In particular, the lack of ability to remove inlet impaction artifacts that are presumably pure Al alloys or pure SiO_x (glass?) hampers the identification of crustal material as IPR and complicates the interpretation of the Biominsal category. The study would benefit from a more refined analysis of artifacts that considers internal versus external mixtures, particle size, and a presentation of example spectra, and a lab study that generates artifacts from the inlet materials.

With regard to the results presented in Worringer et al. (2015) (now published in final version in ACP) three types of artifacts are possible: Si-O spheres with a size of approximately 1 μm sampled with the ISI, Al-O particles (probably aluminum oxides/hydroxides) measured by the use of the Ice-CVI as well as lead-bearing particles. SEM inspection of the surface of the impaction plates revealed the presence of large ($> 1 \mu\text{m}$), homogeneous Pb-rich particles. We did not measure such particles with the ALABAMA. All lead-containing particles detected by ALABAMA are a mixture of lead and other material, also those particles with a size larger than 1 μm .

Due to the fact that we measured only one polarity (cations) we cannot estimate whether we sampled Si- and Al-O. But we measured no particle mass spectra showing a single peak at m/z 27 or m/z 28. However, in order to exclude any possible influence of aluminum or silicon oxides, m/z 27 and m/z 28 were not used as a marker for mineral particles in the classification of the particles measured while using the Ice-CVI or ISI.

Page 12 line 30 – page 13 line 8.

The observation of Pb-rich particles from only one of the IPR inlets is very suspect. While Pb would be a surprising artifact from inlet materials, internal mixtures with Fe with Cr (and Mo??) may also indicate stainless steel artifacts. The authors mention the Worringer paper that describes Pb artifacts from EM analysis (p.4692). However, they do not adequately explain the source of the Pb-rich particles in their analysis or that they are different than in Worringer. Weren't the EM sampler and ALABAMA sampling from the same inlet(s) and thus subject to the same artifacts? It is not adequate to state that the P-rich particles detected by ALABAMA were not the same as those in metals (possibly indicative of inlet materials, particularly brazing or soldering). Also, I do not understand the origin of the Pb-rich particles (1.22) that "might be artifacts from mechanical resuspension". Are the authors suggesting that these Pb-rich particles were previously impacted on the Ice-CVI?

The Pb-containing particles, which were classified as artifacts with respect to their morphology and size (see ACP version of Worringer et al., 2015) were probably produced while ice particles bounced off the impaction plates of the Ice-CVI and removed some material. Some parts of the Ice-CVI are manufactured from Pb-containing aluminum alloy. The Pb-containing particles we have measured using the Ice-CVI as well as using the total inlet consist of Pb plus organic material mixed with minerals and/or salts and "industrial metals" like Fe, Mn, V and Cr. We saw no Pb-containing particles mixed only with other heavy metal signals. All particles showing heavy metal signals are mainly mixed with organic material. Because of these mixing type we assume, that these particles do not originate from contaminations of the stainless steel tubes. Particles which are artifacts from stainless steel tubes were also expected to occur directly after switching the valve. This is also not the case. All particles were measured somewhere in the middle of each event. The fact that no lead containing particles were measured while using the ISI can only be explained with different air masses and different aerosol composition. Parallel measurements behind the two different inlet systems were not possible during the Jungfrauoch 2013 campaign.

Page 14 line 18 – 25.

The authors need to explain the inconsistent Pb signatures, perhaps by investigating subpopulations of category 1d further, and reconcile these results with that of the Worringer paper that presents Pb artifacts from the EM analysis. If this cannot be accomplished, the discussion of Pb-rich particles should be removed.

See reply to comment above.

2) Compositional categories.

The analysis is constrained by the results of the clustering algorithm, which is not separating compositional classes as well. Some classes (1b and 1c) are very similar, whereas other classes probably contain distinct subpopulation. In this way the single-particle nature of the data is not well used. The authors employ the clustering results without further refinement. While this is understandable as a semi-objective approach, the lack of further refinement or analysis based on chemical knowledge and compositional information fundamentally limits interpretation of the results and overall impact of the study. The authors should consider further analysis, which may include allowing additional clusters, refining clustering parameters, and investigating sub-classes.

We strongly disagree with the statement “The authors employ the clustering results without further refinement”. The clustering procedure was done as follows:

As already explained, for our data evaluation we used the fuzzy c-means algorithm. The result of the clustering is highly dependent on the chosen initial number of clusters. If this initial number of clusters is too small, some cluster types may not be found. Therefore we chose a high number of clusters. In the case of the background aerosol (71064 spectra) we started the first clustering with 200 clusters. Each of the resulting 200 clusters was manually inspected, and based on its ion signatures it was assigned to one particle type. Those spectra that cannot be sorted by the algorithm into one of the 200 clusters (membership coefficient below a pre-defined threshold) are assigned to a “rest cluster” (12407 spectra in the case of the background aerosol). This rest cluster was clustered again with a reduced condition for the cluster difference and with an initial number of clusters of 25.

The number of cluster was still too large after the clustering of the “rest cluster”, so it was further analyzed. First, the remaining spectra were sorted by the use of specific marker peaks and the resulting clusters were then clustered again with changing the fuzzyfier from 1.2 to 1.3 and a cluster difference of 0.7. After that, the resulting clusters were manually inspected and sorted (with the criterion $r^2 \geq 0.7$). By this, we could reduce the number of spectra in the rest cluster from 12407 to 3243. Due to this sorting procedure based on both automatic clustering and manual cluster inspection one particle type typically contains different clusters with different fragmentations. For example, the particle type “organic carbon” includes clusters showing aliphatic hydrocarbon, aromatic carbon, nitrogen and oxidized carbon fragmentation patterns. In order to restrict the result to a reasonable number of particle types, we summarized these clusters to one particle type.

We explained the clustering procedure in detail in the appendix.

Fig 1b (Organic carbon) and 1c (BC with organic carbon) have nearly identical average spectra, the only difference being intensity of the K⁺ peak and an NH₄⁺ peak in 1b. The C_n/C_nH_x ratios are not consistently higher in the 1c BC/OC category, so what suggests that these have higher BC content? This appears to be an example of how clustering algorithm is separating spectra based on the dominant signature (K⁺), despite that 1b and some of 1c belong to the same broad compositional class. The K⁺ signal clearly identifies 1b as having a biomass burning origin. (see also Hudson JGR 2004). 1b is labeled somewhat generally as Organic Carbon. This labeling is a little misleading and causes problems later where the authors state, “the data indicate that organic material dominates the IPR composition...” (4693, line 21), citing the 1b category but neglecting that these BB particles also contain BC and inorganic material (K, Na, associated anions), which may be important for ice nucleating. Also p.4699 1.9. 1c (BC/OC) is probably a mixture of BB and other types and is therefore difficult to interpret. Can 1c be more clearly separated from 1b using different clustering parameters?

The difference between 1b and 1c is the more distinct C_n⁺-pattern (m/z 36, 48, 60) in Fig. 1c and not the intensity of the K-peak or the absence of ammonia. Because we measured only cations we cannot unambiguously classify those particles as biomass burning particles and we do not consider just a large peak at m/z 39 mixed with elemental and aliphatic carbons as sufficient evidence for biomass burning. The OC type includes different types of organic fragmentation (aromatics, nitrogen and oxidized carbon). Because we cannot clearly assign these different types of fragmentation to one source we determined to summarize these spectra to these two particle types without including a particle origin.

Later in the Results section the authors discuss BB particles and state that K⁺ was present in nearly every BC, BC/OC, OC mass spectrum (or can it be C₃H₃⁺?), with the K⁺ appearance being consistent across the different sampling inlets. It is therefore not clear why the authors state on p.4695 line 9 that these spectra cannot be clearly assigned to BB or biological particles. Certainly the authors can invoke knowledge from their previous field studies and/or use other BB tracers to confirm the particles' identities. Provided this assumption is true, would some of the BB text and identification be better placed in section 2, and the categories labeled appropriately? Several conclusion about the origin of particulate organic material at the sampling site can be made here but are not discussed (wintertime biofuels, power generation, comparison to previous JFJ studies, etc).

The fragment C₃H₃⁺ and potassium have the same m/z. Because of having no high resolution mass spectrometer we cannot distinguish between both. It is possible that m/z 39 results from the fragment C₃H₃⁺. But potassium is very easy to ionize, thus it is unlikely that C₃H₃⁺ is dominating the mass spectrum.

But, as already stated above, potassium occurs in nearly every organic mass spectrum, and thus it would be too speculative to assign almost all organic aerosol particles to a biomass burning source.

We shifted the paragraph discussion of possible biomass burning origin to section 2.6.

As the authors state, the BioMinSal is not clearly defined category, and is therefore problematic to this study. There is too much speculation here, and this category requires further analysis to be presented at all. The last thing the literature needs is another SPMS paper reporting possible biological material based on weak analysis. In fact, the authors state in the conclusion (p. 4699 l. 15) “we conclude and confirm a better ice nucleation ability for ...biological particles”. This statement is not supported by the SPMS data as presented, and much more careful validation in the laboratory and/or by other bio-specific measurement techniques is required. BioMinSal could possibly be split into multiple categories or at least the populated spectra should be analyzed further. For instance, aluminum is a dominant marker in the cluster and is clearly indicative of crustal material and not biological material, yet it is not mentioned. The authors do concede that Al and Si are possible inlet contaminants, but it is unclear how widespread and in what form that contamination is observed (can Al contamination really be observed as an internal mixture in submicron particles?). What % of the spectra contain Al, from both inlets? Iron is not labeled and very hard to see in the figure – is it really Fe or CaO? The authors claim to observe the ^{54}Fe isotope, yet they state 56 could be due to ions other than Fe, thus some inconsistency. Fe may be an unusual/minor marker for biological material (no clear consensus in the literature). The authors’ suggestion of hemoglobin as the Fe source would necessitate animal cellular material and is highly speculative without including references. Other strong unlabeled signals appear to be nitrogen oxides and phosphorus, which is inorganic phosphate from minerals or may possibly be a biological marker.

*In our conclusion, we confirm a better ice nucleation ability for larger, primary aerosol particles **such as** minerals, salts and biological particles, because of the higher relative number of larger particles in the IPR composition as in the background aerosol. We did not mean to say, that the particle type “BioMinSal” definitely contains biological particles. In the present analysis the “BioMinSal”-type contains particle mass spectra that show only (single) metal peaks, like m/z 39 alone or in combination with m/z 23. Without anions, the origin of these particle types cannot be clearly classified. Laboratory studies show that the origin could be either salts, crustal material **or** biogenic material. To make this more clear, we renamed this particle type to Bio/Min/Sal. It should also be emphasized that the average mass spectrum of this particle type shows many ion signals, but not the individual mass spectra. Therefore it is not possible with this data set to split the “Bio/Min/Sal” category into further subgroup.*

Aluminium (m/z 27) is detected in some spectra, however not as single signal, but mostly in combination with sodium and potassium. About 18% of the spectra assigned to the Bio/Min/Sal-type in the IPR include aluminum (m/z 27) and 5% of the background aerosol. As mentioned before, to minimize the risk of artifacts particle influencing the particle classification, Al was not used for assigning IPR to the particle type “minerals”.

The peak at m/z 56 was assigned to Fe, only if also the isotope at m/z 54 was present. Otherwise, if Ca (m/z 40) is present, m/z 56 is assigned to CaO. If the rest of the mass spectrum contains a lot of organic signals, m/z 56 may also be a fragment of an organic substance. Laboratory studies conducted in our lab showed that mass spectrum of hemoglobin particles show a signal at m/z 56.

We agree with the statement that phosphorous can be inorganic phosphate from minerals or may possibly be a biological marker, but this strengthens our decision to assign particles to the “Bio/Min/Sal” group when no clear assignment to a certain source is possible.

Page 10 line 11 – 25.

The BC category is only presented for the background aerosol in Fig 8, and is absent for all IPR data in Fig 2, 4, and 8. Was this category manually incorporated into the BC/OC category, or did this category simply have zero population? If the latter, then add the BC category to the legends of Fig 2 and 4. Also, this is an important scientific point. Please discuss the lack of BC in IPR. The authors state (p. 4692 l. 13) “an enrichment of BC is not observed in our measurements”, but in the conclusions (p.4699 l. 25) they also state that this study describes “BC as a good ice nuclei”. Please fully clarify the analysis and ensure the conclusions are consistent with the data.

It is really the case that no pure BC particles were found in the IPR composition. We added the BC-type in the legends of Fig 2 and 4 and include it in the IPR composition as zero population. We mentioned this finding in the discussion (p. 4699, l. 24), but we state there “These results comply with previous investigations (DeMott et al., 1999; Dymarska et al., 2006; Hoose and Möhler, 2012) describing black carbons as a good ice nuclei but only at lower temperatures”.

Thus, the finding that BC is a good ice nucleus was cited from other studies, and we also emphasize that this finding holds for low temperatures. In our case temperatures were higher, and this may be the explanation for not detecting BC in the IPR.

Minor comments

Section 2.3. What fraction of droplets <5 microns are not impacted on the preimpactor and thus make it through the CVI and can be observed as IPR? This has to do with the sharpness of the preimpactor transmission curve, and Mertes 2007 can be referenced if those data can be applied to the cloud conditions under study here. This is important because in mixed phase clouds ~5 micron droplets can be much more abundant than ~5 – 20 micron crystals such the IPR analysis would be dominated instead by droplet residues. Also, do >20 micron crystals bounce upon impact in the omni-directional inlet (and therefore remain in the sample flow), similar to the designed bounce that happens in the preimpactor?

No droplets < 5 μm are impacted in the pre-impactor and thus remain at this point in the sample flow. But these small droplets are removed a little later by the CVI itself, because its lower cut-off of is at 5 μm , i.e. that all droplets are pre-segregated by using the combination of pre-impactor and CVI. Of course, the transmission curves of the pre-impactor as well as the CVI have a different sharpness, but they overlap sufficiently so that no residuals of droplets are observed behind the Ice-CVI as demonstrated in Mertes et al. (2007). The whole issue is now described in much more detail in section 2.3 of the revised manuscript. Page 6 line 24 – 32.

Indeed, it might be possible that particles > 20 μm bounce upon impact in the inlet and would remain in the sample flow first. But for those cases or if ice particles > 20 μm are directly

aspirated by the inlet without bouncing before, there is a virtual impactor installed downstream the inlet within the modular Ice-CVI system that removes all particles larger than 20 μm , i. e. they are removed from the sample flow by the virtual impactor (btw. before they reach the pre-impactor). This is already explained in the first part of section 2.3.

It is a very distinct compositional category but labeling it as “industrial metals” is too general and possibly erroneous. See Jang AE 2006, Ault EST 2010, Sodeman EST 2005, Lake AE 2004, many others.

The particle type “industrial metals” includes a mixture of different kinds of heavy metals like iron, manganese, chromium and vanadium. Because of the lack of the anions we cannot clearly estimate the source of these particles. Contaminations from the stainless steel tube can be mostly excluded, because they were not sampled directly after switching the valve. “Anthropogenic metal-containing particles” might also be a suitable classification.

Page 11 line 3 – 9.

The compositional categories in Fig 9 are not consistent with the rest of the paper.

This was intended to show more precisely the differences in the chemical composition regarding to the air mass origin. Otherwise there would have been only three particle types with nearly the same number of particles.

Sulfate and nitrate are likely to account for a significant mass fraction of submicron aerosol. Are these compounds detected by ALABAMA, and in which categories?

As mentioned several times, anions were not detected during the Jungfraujoch study due to a technical problem. Therefore sulfate and nitrate (detected via NO_2^- , NO_3^- , and SO_2^- , SO_3^- , HSO_4^-), respectively, were not measured during this study.

Consider presenting spectra intensities on a log scale so that important minor contributions are not hidden. Many of the signatures described in 2.6 cannot be seen in the mass spectra. Isotope signatures as ^{54}Fe are not clear.

Figure 1 shows only an averaged spectra for each particle type. In section 2.6 it is described which marker peaks are used to assign one mass spectrum to one of these seven particle types. Not every mass spectrum shows all mentioned marker peaks.

The logarithmic scale shows no new insights regarding to the marker peaks.

p.4690 l 15. How were periods of contamination by secondary ice and snowflake fragments identified?

Periods of contamination by secondary ice and ice crystal fragments cannot be identified, but a possible contamination cannot be ruled out in case of blown snow and precipitation. That is the reason that cloud periods are distinguished in (++)- and (+-)-events, which is now explained in more detail in the revised version (Page 12 line 16 – 26). Due to closer consideration of the (++)- and (+-)-events and taking into account that the ALABAMA did

not measure the whole cloud event at the Ice-CVI we get a new classification with more (++)-events which are now called (++)/(-)-sampling-periods (Table 1).

Fig 6 – what does the black lines denote?

The black lines in Fig 6 denote the events with different air mass origin described in Section 3.4. This was explained in the figure caption, but we added “discussed in section 3.4” to the caption for clarity.

In the discussion of lead-containing particles (p.4694 l. 20), the authors cite disagreement between their ambient results and literature studies. However, the comparison is critically dependent on how the various groups identified lead-containing particles. In the current manuscript, it appears only particles where lead is a major ion are included in this category, whereas other groups may use very different criteria.

We classified a mass spectrum as lead-containing particle if the lead pattern is obviously seen and is clearly distinct from the noise. Also Kamphus et al. (2010) only assigned particles into the “lead” type when the isotopes at m/z 206 and 208 were visible. Thus it can be assumed that the criteria in both cases are similar.

In the comparison of size distributions (p. 4697), the authors mention that ALABAMA (and ESEM – really?) has a size-dependent detection efficiency. This should be considered when stating that agreement between measurements is “very good” or otherwise. Likewise, the particle density could play a significant role comparing vacuum aerodynamic with geometric diameter, eg, in Fig 10a. The y-axes for Fig 10 a, c, e are labeled $dN/d\log D$, but I suspect this is incorrect since no units are given and there is no mention of how obtain quantitative size distribution from ALABAMA. Were the data normalized and if so how? Please be clear. What is the reason for 2 order magnitude drop in OPC concentration over 1 bin in 10d? Typo in caption: 3 μm

The data were normalized to the highest number concentration, but the number per size closes were divided by $d\log$ (Zimmermann et al., 2003), such that the unit is correct. We labeled all axes “ $dN/d\log d$, normalized”. Geometric diameters obtained from ESEM were converted to vacuum aerodynamic diameter. An explanation was added to the manuscript: Page 19 line 8 – 19.

The typo was corrected.

Fig 11. The authors present statistical differences between background aerosol and IPR for the OPC and Biominsal categories, but these principal results are presented with essentially no interpretation or context (p. 4698).

We assume that the reviewer means “OC and Biominsal” categories.

We have extended the discussion of Figure 11 (in section 3.5) as follows: Page 20 line 15 – page 21 line 2.

Figure 11 shows the chemical composition of the IPR and background aerosol particles larger than 1 μm . The most frequent particle types found in the IPR larger than 1 μm are OC,

lead containing particles, Bio/Min/Sal, and minerals for the Ice-CVI, and Bio/Min/Sal and minerals for the ISI. Lead containing particles are found in the IPR sampled by the Ice-CVI to a similar percentage (14 %) as in all IPR (7 %, see Figs. 2 and 8). Interestingly, the background aerosol supermicron particles are dominated by the Bio/Min/Sal-type and OC. The finding strengthens the assumption that the metal ions detected in these mass spectra are likely metal cations of primary aerosol like sea salt, minerals or biological particles, which are mainly found in the coarse mode (e.g., Seinfeld and Pandis, 2006). Such large primary particles are also expected to act efficiently as INP, and it is therefore not surprising that they are found in the supermicron IPR. More surprising is the large fraction of OC and BC/OC particles detected in the supermicron IPR. These large particles containing organic material appear to be even better INP than the supermicron particles assigned to the Bio/Min/Sal category. It has recently been suggested that porous and glassy organic particles under certain conditions play an important role as INP (Murray et al., 2010; Adler et al., 2013), and this may explain the results presented here. But also the origin of these supermicron organic particles remains unclear. Primary biological material as a source for these particles is regarded to be unlikely, because the marker peaks observed in cations of biological particles (like K^+ , Na^+ , Ca^{2+}) were not observed in these particle spectra assigned to the OC and BC/OC types. However, particle classification of single particle mass spectra is never absolutely certain, and future work may reveal more insight into the nature and origin of these particles.

Reference formatting is not consistent. Sometimes “et al.” is omitted. Differentiate between the two Cziczo et al. 2004 papers.

This has been corrected.

Wording and phrasing: p. 4685 l. 15 and 18. “released”

Not clear what is meant here.

p. 4688 l. 23

“unambiguous” was changed to “unambiguously”

Page 11 line 12.

p. 4692 l. 7

We changed the sentence to “The air masses during the (++)-events came primarily from north-western directions from North America over France, while during the (+-)-events the air masses arrived more from the North, over Scandinavia and Germany”.

Page 14 line 5 – 8.

p. 4692 l. 17 verb tense

We changed the verb tense. Page 14 line 17.

p. 4698 l. 13

This paragraph was replaced. See comment above page 20 line 15 – page 21 line 2.

p. 4699, l. 11

We changed the sentence to “Besides, the “minerals” group was found to be one of the main fractions of the IPR measured behind the Ice-CVI”.

Page 21 line 29/30.

p. 4702 l. 10&12

We changed “whereby” to “where” in line 10, but we do not know what is wrong in line 12.

Page 24 line 2/3.

Adler, G., Koop, T., Haspel, C., Taraniuk, I., Moise, T., Koren, I., Heiblum, R. H., and Rudich, Y.: Formation of highly porous aerosol particles by atmospheric freeze-drying in ice clouds, *Proceedings of the National Academy of Sciences of the United States of America*, 110, 20414-20419, 2013.

DeMott, P. J., Chen, Y., Kreidenweis, S. M., Rogers, D. C., and Sherman, D. E.: Ice formation by black carbon particles, *Geophysical Research Letters*, 26, 2429-2432, 1999.

Dymarska, M., Murray, B. J., Sun, L., Eastwood, M. L., Knopf, D. A., and Bertram, A. K.: Deposition ice nucleation on soot at temperatures relevant for the lower troposphere, *Journal of Geophysical Research-Atmospheres*, 111, D04204, 2006.

Hoose, C., and Möhler, O.: Heterogeneous ice nucleation on atmospheric aerosols: a review of results from laboratory experiments, *Atmospheric Chemistry and Physics*, 12, 9817-9854, 2012.

Kamphus, M., Ettner-Mahl, M., Klimach, T., Drewnick, F., Keller, L., Cziczo, D. J., Mertes, S., Borrmann, S., and Curtius, J.: Chemical composition of ambient aerosol, ice residues and cloud droplet residues in mixed-phase clouds: single particle analysis during the Cloud and Aerosol Characterization Experiment (CLACE 6), *Atmospheric Chemistry and Physics*, 10, 8077-8095, 2010.

Murray, B. J., Wilson, T. W., Dobbie, S., Cui, Z., Al-Jumur, S. M. R. K., Möhler, O., Schnaiter, M., Wagner, R., Benz, S., Niemand, M., Saathoff, H., Ebert, V., Wagner, S., and Kärcher, B.: Heterogeneous nucleation of ice particles on glassy aerosols under cirrus conditions, *Nature Geoscience*, 3, 233-237, 2010.

Seinfeld, J. H., and Pandis, S. N.: *Atmospheric Chemistry and Physics: From Air Pollution to Climate Change*, John Wiley & Sons, Inc., New Jersey, 2006.

Worringen, A., Kandler, K., Benker, N., Dirsch, T., Mertes, S., Schenk, L., Kästner, U., Frank, F., Nillius, B., Bundke, U., Rose, D., Curtius, J., Kupiszewski, P., Weingartner, E., Vochezer, P., Schneider, J., Schmidt, S., Weinbruch, S., and Ebert, M.: Single-particle characterization of ice-nucleating particles and ice particle residuals sampled by three different techniques, *Atmospheric Chemistry and Physics*, 15, 4161-4178, 2015.

Zimmermann, R., Ferge, T., Galli, M., and Karlsson, R.: Application of single-particle laser desorption/ionization time-of-flight mass spectrometry for detection of polycyclic aromatic hydrocarbons from soot particles originating from an industrial combustion process, *Rapid communications in mass spectrometry* : RCM, 17, 851-859, 10.1002/rcm.979, 2003.

In-situ single submicron particle composition analysis of ice residuals from mountain-top mixed-phase clouds in Central Europe

S. Schmidt¹, J. Schneider¹, T. Klimach¹, S. Mertes², L. P. Schenk², J. Curtius³, P. Kupiszewski⁴, E. Hammer^{4*}, P. Vochezer⁵, G. Lloyd⁶ M. Ebert⁷, K. Kandler⁷, S. Weinbruch⁷, and S. Borrmann^{1,8}

[1]Particle Chemistry Department, Max Planck Institute for Chemistry, 55128 Mainz, Germany

[2]Leibniz Institute for Tropospheric Research, 04318 Leipzig, Germany

[3]Institute for Atmospheric and Environmental Sciences, Goethe-University of Frankfurt am Main, 60438 Frankfurt, Germany

[4]Laboratory of Atmospheric Chemistry, Paul Scherrer Institute, 5232 Villigen, Switzerland

[5]Institute for Meteorology and Climate Research, Karlsruhe Institute of Technology, 76021 Karlsruhe, Germany

[6]School of Earth, Atmospheric & Environmental Science, The University of Manchester, M13 9 PL Manchester, United Kingdom

[7]Environmental Mineralogy, Institute of Applied Geoscience, Technical University Darmstadt, 64287 Darmstadt, Germany

[8]Institute for Atmospheric Physics, Johannes Gutenberg University, 55128 Mainz, Germany

* now at: Grolimund + Partner AG – environmental engineering, 3018 Bern, Switzerland

Correspondence to: S. Schmidt (susan.schmidt@mpic.de)

Abstract

Ice nucleating particles have a high impact on ice crystal formation in clouds and thereby on precipitation and the global radiation budget. Because the chemical composition of these particles plays an important role at the nucleating processes, investigation of the chemical composition of ice nucleating particles is a topic of current research. This paper presents results from the “INUIT/CLACE 2013” (Cloud and Aerosol Characterization Experiment) field campaign at the high alpine research station Jungfraujoch in January/February 2013. The chemical composition of ice particle residuals (IPR) was measured in orographic, convective and non-convective clouds. The submicron particles were analyzed by a single particle mass

1 spectrometer (ALABAMA) under ambient conditions characterized by temperatures between
2 $-28\text{ }^{\circ}\text{C}$ and $-4\text{ }^{\circ}\text{C}$ and wind speed from 0.1 m s^{-1} to 21 m s^{-1} . Additionally, background aerosol
3 particles in cloud free air were investigated. The IPR were sampled from mixed-phase clouds
4 with two inlets which selectively extract small ice crystals in-cloud, namely the Counterflow
5 Virtual Impactor (Ice-CVI) and the Ice Selective Inlet (ISI). The IPR as well as the aerosol
6 particles were classified into seven different particle types: (1) black carbon, (2) organic
7 carbon, (3) black carbon internally mixed with organic carbon, (4) minerals, (5) one particle
8 group (termed “Bio/Min/Sal”) that may contain biological particles, minerals, or salts, (6)
9 industrial metals, and (7) lead containing particles. For any sampled particle population it was
10 determined by means of single particle mass spectrometer how many of the analyzed particles
11 belonged to each of these categories. Accordingly, about 30 % of the IPR and roughly 43 %
12 of the background particles contained organic carbon. The measured fractions of minerals in
13 the IPR composition varied from 10 % to 14 %, while the values for the “Bio/Min/Sal” group
14 were between 20 % and 54 %. Two percent to 20 % of the IPR contained organic carbon
15 mixed with black carbon. Both inlets delivered similar results of the chemical composition
16 and of the particle size distribution, although lead was found only in the IPR sampled by the
17 Ice-CVI. The results show that the ice particle residual composition varies substantially
18 between different cloud events, which indicates the influence of different meteorological
19 conditions, such as origin of the air masses, temperature and wind speed.

20

21 **1 Introduction**

22 Ice formation in clouds influences the life-time of clouds, the formation of precipitation, and
23 the Earth’s solar and thermal radiation budget (Lohmann and Feichter, 2005). There are two
24 major pathways by which ice is formed in the atmosphere: homogeneous and heterogeneous
25 freezing. The spontaneous formation of ice inside droplets at temperatures of lower $-37\text{ }^{\circ}\text{C}$
26 and without any catalysts is called homogenous freezing (Cantrell and Heymsfield, 2005) and
27 occurs in high clouds at a saturation similar to that of liquid water (Koop et al., 2000).
28 Heterogeneous freezing needs particulate catalysts to initiate freezing at temperatures higher
29 than $-37\text{ }^{\circ}\text{C}$ in mixed-phase clouds. These catalysts are called ice nucleating particles (INP).
30 There are four different heterogeneous ice formation modes (Pruppacher and Klett, 2010):
31 deposition nucleation, condensation freezing, immersion freezing and contact freezing.
32 Because heterogeneous freezing starts at higher temperatures than homogeneous freezing, ice
33 crystals, which are formed by ice nucleating particles grow faster (by diffusion) and perhaps
34 precipitate first (DeMott et al., 1998). Another reason for faster formation of precipitation is

1 the Wegener-Bergeron-Findeisen process, which plays an important role on cloud formation
2 and precipitation, especially in mixed-phase clouds. In mixed-phase clouds, where
3 supercooled droplets and ice crystals exist, the supercooled droplets evaporate and the water
4 vapor freezes on the ice crystals. Because of the lower saturation vapor pressure over ice than
5 over water the ice crystals will grow at the expense of cloud droplets. This results in a quick
6 freezing of the supercooled water cloud. These iced clouds have a shorter lifetime than
7 supercooled water clouds, because the precipitation formation via the ice phase is more
8 efficient than in warm clouds (Lohmann and Feichter, 2005).

9 Ice formation is very selective because of the low number concentration of particles that can
10 act as INP. Roughly about one in 10^5 atmospheric particles can act as INP (Rogers et al.,
11 1998; DeMott et al., 2010). The ice nucleation is induced at some point on the surface of the
12 nucleating particle and the ice nucleation ability of different types of aerosol particles is
13 usually described either by an ice active-site density approach or by classical nucleation
14 theory involving a contact angle (see e.g. Steinke et al., 2015, and references therein). Several
15 laboratory, field and model studies (DeMott et al., 2003a; DeMott et al., 2003b; Cantrell and
16 Heymsfield, 2005; Kamphus et al., 2010; Hoose et al., 2010; Hartmann et al., 2011; Murray et
17 al., 2011; Hoose and Möhler, 2012; Murray et al., 2012; Atkinson et al., 2013; Diehl et al.,
18 2014) have shown that certain mineral dusts belong to the most important ice nucleators in the
19 atmosphere because of their high abundance. On the other hand, biological particles like
20 bacteria, pollen and spores (e.g. Diehl et al., 2001; von Blohn et al., 2005; Möhler et al., 2007;
21 Pratt et al., 2009; Prenni et al., 2009; Diehl and Wurzler, 2010) are the most efficient ice
22 nuclei (Hoose et al., 2010). Also soot (e.g. Cozic et al., 2008a; Pratt and Prather, 2010; Pratt et
23 al., 2010) and effloresced salts (Abbatt et al., 2006; Wise et al., 2012) have been found to act
24 as ice nuclei. There is also some evidence that glassy organics (Froyd et al., 2010; Murray et
25 al., 2010), porous particles (Adler et al., 2013) and lead-containing particles (Cziczo et al.,
26 2009; Ebert et al., 2011) have favorable ice nucleation qualities.

27 Direct measurements of the chemical composition of single INP or IPR (Ice particle residuals
28 = particles remaining after the ice of cloud ice particles is evaporated) are important to better
29 understand ice formation in mixed-phase clouds, to improve the prediction of precipitation,
30 and to evaluate the influence of anthropogenic aerosol on these processes. Measurements of
31 INP/IPR require instrumentation that can separate the INP/IPR from the background or
32 interstitial aerosol particles and supercooled drops and measure the chemical composition on-
33 line. In several field studies a combination of a CFDC (Continuous Flow Diffusion Chamber;

1 Chen et al., 1998), a CVI (Counterflow Virtual Impactor; Cziczo et al., 2003; Mertes et al.,
2 2007) which separates the ice crystals from background aerosol and a Single Particle Mass
3 Spectrometer (SPMS; DeMott et al., 2003a; Cziczo et al., 2003; Cziczo et al., 2004a; Cziczo
4 et al., 2004b; Pratt et al., 2009; Corbin et al., 2012) to measure ice nucleating particles were
5 deployed. Previous measurements of INP and IPR (on-line and off-line) conducted at the
6 Jungfraujoch showed that particles consisting of mineral components dominate the ice
7 particles number (Kamphus et al., 2010), but also particles containing black carbon (Mertes et
8 al., 2007; Cozic et al., 2008a) and lead (Cziczo et al., 2009; Ebert et al., 2011) were found to
9 be enriched in IPR.

10 Here we report on measurements conducted with the single particle instrument ALABAMA
11 (Aircraft-based Laser Ablation Aerosol Mass Spectrometer; Brands et al., 2011) to analyze
12 the chemical composition of IPR sampled by two unique different ice sampling inlets. The
13 goal of these measurements was to investigate the chemical composition of IPR in ambient
14 mixed-phase clouds in upward transported boundary layer air and free tropospheric air at the
15 high-alpine research station Jungfraujoch (JFJ; 3580 m asl) in Central Europe. Additionally,
16 background aerosol was measured by the use of a total inlet during cloud free conditions.

17

18 **2 Experimental**

19 **2.1 Measurement location and meteorological conditions**

20 The intensive field campaign INUIT-JFJ/CLACE 2013 in January/February 2013 at the High
21 Alpine Research Station Jungfraujoch (JFJ, Swiss Alps; Sphinx Laboratory, 3580 m asl;
22 7°59'2''E, 46°32'53''N) took place in the framework of the DFG (Deutsche
23 Forschungsgemeinschaft)-funded research unit INUIT (Ice Nuclei research UnIT) and the
24 Swiss National Science Foundation-funded *Interaction of aerosols with Clouds and Radiation*
25 *project* (see also overview paper by Schneider et al., this issue). The IPR were sampled out of
26 mixed-phase clouds by the Ice-CVI (Ice Counterflow Virtual Impactor; Mertes et al., 2007)
27 and the ISI (Ice Selective Inlet; Kupiszewski et al., 2014) and fed into the ALABAMA single
28 particle mass spectrometer (Brands et al., 2011). During cloud free times the ALABAMA was
29 connected to the heated total inlet (20 °C; Weingartner et al., 1999) to sample the background
30 aerosol particles. The Ice-CVI and the total inlet were located in a central position on the roof
31 of the Sphinx Laboratory and the ISI was located at the railing at the eastern edge of the roof.
32 A short description of the instruments is given in Sections 2.2 to 2.5. Both the Ice-CVI and
33 ISI sample only ice crystals smaller than 20 μm. Such small ice crystals have grown only by

1 water vapor diffusion and have an age of less than about 20 seconds (Fukuta and Takahashi,
2 1999). It is therefore very likely that these ice crystals have formed in the vicinity of the inlets
3 and that the IPR extracted from such fresh ice crystals corresponds to the original IPN. The
4 meteorological conditions during the campaign along with basic information on the
5 encountered cloud types are summarized in Table 1.

7 **2.2 ALABAMA (Aircraft-based Laser Ablation Aerosol MAss spectrometer)**

8 The ALABAMA (Brands et al., 2011) consist of three sections: aerosol inlet, sizing region
9 and desorption/ionization region. The aerosol inlet is an aerodynamic lens (Liu-type; Liu et
10 al., 1995b; Liu et al., 1995a; Liu et al., 2007; Kamphus et al., 2008) which focuses aerosol
11 particles to a narrow beam by utilizing 6 apertures with decreasing diameter. The particles are
12 separated from ambient air and accelerated to $50 - 100 \text{ m s}^{-1}$, while entering the vacuum-
13 system. For optimal sampling conditions the pressure in front of the aerodynamic lens should
14 be between 0.5 hPa and 5 hPa. For this, a critical orifice is used, which limits the flow to
15 $80 \text{ cm}^3/\text{min}$ under standard working conditions and which reduces the pre-pressure of the lens
16 to 3.8 hPa. During this campaign, the critical orifice was constructed by a constricted O-ring
17 such that also under Jungfraujoch conditions (ambient pressure around 630 hPa) the lens
18 pressure was regulated to best operating conditions. A skimmer separates the first and the
19 second pumping stages. Two continuous wave detection lasers, which are orthogonal to the
20 particle beam, are located in the second pumping stage. As a modification of the instrument
21 described in Brands et al. (2011), two UV laser diodes (Blu-Ray laser; InGaN, 405 nm) are
22 now used. The particles pass through the laser beams and the scattered light is reflected by an
23 elliptical mirror and detected by a photomultiplier tube (PMT). The vacuum aerodynamic
24 particle size (DeCarlo et al., 2004) can be determined from the velocity of the particles by
25 calibration with particles of known size. In this section the ablation laser (pulsed Nd-YAG-
26 Laser, 266 nm; 6 – 8 mJ per pulse, 5.2 ns per pulse, max. 21 Hz) is triggered. If one particle
27 passes through both laser beams, the in-house designed and built electronic control system
28 sends out a trigger signal to the ablation laser, the laser shoots and ionizes the particles. The
29 ions are separated in the Z-shaped bipolar time-of-flight mass spectrometer (TOFWERK AG,
30 Switzerland) by their mass-to-charge ratio. In principle both signals (for positive and negative
31 ions) can be detected using a multichannel plate (MCP). However, for this study only positive
32 ions were available due to technical issues. The average mass resolution $m/\Delta m$ of the Z-ToF
33 mass spectrometer ranges between 100 for low m/z values and 200 for larger ions (Brands et
34 al., 2011). The ALABAMA covers a size diameter range from 100 to 3000 nm (see Fig. 10)

1 with the most efficient size diameter range being between 200 nm and 900 nm. Particles in the
2 size diameter range of approximately 400 nm were ionized at best.

3 Additionally the particle size distribution was measured by a Sky-OPC (Optical Particle
4 Counter; Grimm 1.129) with size diameter range from 0.25 to 52 μm . The Sky-OPC is
5 integrated into the ALABAMA instrument upstream of the aerodynamic lens. Due to the size
6 limitation by the inlet system a maximum particle size of approximately 3 μm was measured.
7 Both instruments sampled through ¼" stainless steel tubes with different lengths (ISI =
8 370 cm; Ice-CVI = 126 cm; total = 261 cm). Particle losses inside the sampling tube were
9 calculated with the Particle Loss Calculator (von der Weiden et al., 2009). In the size range
10 between 200 nm and 500 nm the transmission efficiency is about 99 % for all three inlets. The
11 larger the particles and the longer the tubes, the higher are the losses inside the tubes. For a
12 size of 3 μm the transmission efficiency is between 90 % (tube to the Ice-CVI with a length of
13 126 cm) and 45 % (tube to the ISI with a length of 370 cm). The switching between the three
14 different inlets was performed manually.

16 2.3 Ice-CVI (Ice Counterflow Virtual Impactor)

17 The Ice-CVI is designed to sample IPR from mixed-phase clouds. A detailed description and
18 instrumental characterization is provided in Mertes et al. (2007) thus it is only briefly
19 described here. The Ice-CVI uses an omnidirectional inlet, which removes particles larger
20 than 20 μm from the aspired air. The separation of the particles larger than 20 μm out of the
21 sample flow is done with a virtual impactor (VI) downstream of the inlet. After that the
22 supercooled droplets ($> 5 \mu\text{m}$) are removed by a pre-impactor (PI). The PI consists of
23 impaction plates colder than 0 °C. The supercooled droplets freeze on these plates upon
24 contact while the ice crystals bounce off and remain in the sample flow. Subsequently, a
25 counterflow virtual impactor (CVI, Mertes et al., 2005) rejects interstitial aerosol particles,
26 and potentially remaining supercooled drops and ice particles smaller than 5 μm . Thus, all
27 supercooled drops are pre-segregated by the cut-off behavior of PI and CVI and only small ice
28 crystals, i.e. those with aerodynamic size diameters between 5 μm and 20 μm (cut-off
29 properties of VI and CVI) remain in the sample flow. A transmission efficiency of the PI
30 concerning supercooled drops and ice particles of about 0 % and 100 %, respectively, as
31 expected from Tenberken-Pötzsch et al. (2000) and Murphy et al. (2004), was shown by
32 Mertes et al. (2007).

1 For complete sublimation, the small ice particles are injected into particle-free and dry carrier
2 air inside the CVI. The aerosol particles that remain after evaporation/sublimation of the ice
3 are termed IPR. The walls of the evaporation tube as well as the carrier air are at room
4 temperature. The IPR can be transferred to different aerosol instruments for physico-chemical
5 characterization. The sampling principle of the CVI leads to an enrichment of the collected
6 particles. This enrichment (factors between 5 and 10) is given by the ratio of the velocity
7 upstream and downstream the CVI inlet tip.

8 A CPC (Condensation Particle Counter, model 3010, TSI Inc.) was connected downstream of
9 the Ice-CVI at a suitable position for measuring to determine the total particle number
10 concentration of the IPR. Significant non-zero particle number concentrations indicate the
11 presence of ice particles in mixed-phase clouds.

12

13 **2.4 ISI (Ice Selective Inlet)**

14 Extracting IPR from mixed-phase clouds was also possible with the ISI (detailed description
15 in Kupiszewski et al., 2014). Small ice crystals (the IPR within are assumed to be
16 representative of the original ice nuclei) are segregated from larger ice crystals, supercooled
17 droplets and interstitial aerosol particles by a combination of four inlet components. The first
18 component is the omnidirectional inlet, which is shielded from above **in order to prevent** large
19 precipitating particles entering the inlet. Subsequently, a custom-made cyclone (BGI Inc.)
20 removes ice crystals, with aerodynamic diameters of ca. 20 μm (D_{50} cut size, i.e., the particle
21 diameter at which 50 % of incoming particles are removed from the sample flow) and larger.
22 Further downstream the removal of supercooled droplets takes place in a custom built ice-
23 coated droplet evaporation chamber using the Wegener-Bergeron-Findeisen (WBF) process.
24 **The WBF process is used by deploying a chamber with ice-coated inner walls within the ISI,**
25 **thus providing an environment in which there is saturation with respect to ice. This in turn**
26 **means that there is sub-saturation with respect to water (due to the difference in saturation**
27 **vapour pressures over water and ice), which leads to evaporation of liquid droplets inside the**
28 **chamber and transfer of water vapour from the droplets to the ice-coated walls of the**
29 **chamber. The design of the chamber is described in detail in Sect. 2.2 of Kupiszewski et al.**
30 **(2014).** The key difference to the Ice-CVI is that here the separation of supercooled droplets
31 from ice crystals is conducted in the airborne state via evaporation. Finally, the interstitial
32 aerosol and the cloud condensation nuclei (CCN) released during droplet evaporation are
33 removed by a pumped counterflow virtual impactor ($D_{50} \approx 5 \mu\text{m}$). The extracted ice crystals

1 with aerodynamic diameter between 5 μm and 20 μm are heated and the released IPR are
2 transferred into the laboratory for physical and chemical characterization using state of the art
3 single particle aerosol instrumentation (single particle soot photometer (SP2), ALABAMA
4 single particle mass spectrometer, Wideband Integrated Bioaerosol Sensor (WIBS) and a
5 Grimm optical particle counter). The ISI additionally allows for simultaneous counting, sizing
6 and imaging of the hydrometers contained in the cloud with the use of two WELAS (white
7 light aerosol spectrometer; Heim et al., 2008; Rosati et al., 2015) aerosol sensor system (Palas
8 GmbH) and a Particle Phase Discriminator (PPD; Kaye et al., 2008; Vochezer et al., 2015).
9 These are placed behind the cyclone (first WELAS OPSS) as well as behind the droplet
10 evaporation unit (second WELAS OPSS and PPD). The ISI, together with the downstream
11 aerosol instrumentation, thus provides number size distribution of sampled hydrometers and
12 aerosol particles, information on ice crystal shape and surface roughness, as well as number
13 size distribution and chemical composition of ice residual particles.
14 The ISI enriches the collected particles inside the pumped counterflow virtual impactor with
15 an enrichment factor between 1 and 10.

16

17 **2.5 Supplement instruments**

18 **Particle Volume Monitor (PVM; Gerber, 1996):** The PVM measured the liquid water
19 content (LWC = total liquid water present in a cloud) and the surface area of cloud droplets
20 (e.g., Wendisch, 1998). Cloud droplets cross a laser beam and the scattered light is measured.
21 Elevated LWC values are used to identify cloud events, using a threshold value of 20 mg m^{-3} .
22 During the measurement campaign two PVMs were operated by PSI (Paul Scherrer Institute)
23 and the University of Manchester.

24

25 **Cloud Droplet Probe (CDP):** The CDP is a forward-scattering spectrometer for
26 determination of particles sizes and concentrations of cloud droplets. Counting and sizing of
27 the particles is done by detecting light scattered by the particles (for more details see for
28 example Lance et al., 2010).

29

30 **Scanning electron microscopy (SEM):** Ice particle residuals (IPR) were collected by a two
31 stage impactor system (50 % cut-off aerodynamic diameters 1.0 and 0.1 μm , respectively) on
32 transmission electron microscopy grids and elemental boron substrates and analyzed by
33 scanning electron microscopy (SEM, FEI Quanta 200 FEG, FEI Eindhoven, the Netherlands)
34 and energy-dispersive X-ray fluorescence (EDX, EDAX, Tilburg, The Netherlands) to

1 characterize the particles with regard to their chemical composition, morphology, size,
2 internal mixing state and electron beam stability (volatility). (For further details see Kandler
3 et al., 2011). Here we only present the size distribution of IPR measured by SEM and
4 compare them to the IPR sizes obtained by the ALABAMA and the Sky-OPC. Detailed
5 results on the chemical composition analysis of IPR, INP, and background aerosol by SEM
6 are given in Worringen et al., 2015.

7

8 **2.6 ALABAMA data evaluation**

9 The data evaluation was done with the software package CRISP (Concise Retrieval of
10 Information from Single Particles; Klimach, 2012) based on the software IGOR Pro (Version
11 6, WaveMetrics) and following the procedure described in Roth (2014). This software
12 package includes mass calibration, conversion of the mass spectra into ‘stick’ spectra by
13 integration over the peak width, and various procedures to sort the mass spectra into groups or
14 clusters of similar spectra. This sorting can be done manually, by means of cluster algorithms
15 (*fuzzy c-means* or *k-means*), or by searching for certain parameters (e.g., ion signals at a
16 certain m/z ratio).

17 The Clustering depends to some degree on the interstitial settings of the algorithm and its
18 parameters. The start parameters are *Normalization type and time*, *Preprocessing type*,
19 *Initialisation type*, the *number of clusters* and the *start cluster difference*. Using the *fuzzy c-*
20 *means* algorithm (e.g. Bezdek et al., 1984; Hinz et al., 1999; Huang et al., 2013) the
21 parameters *fuzzifier* and *fuzzy abort* have to be set accordingly. The cluster parameters are
22 explained in detail in the appendix.

23 As only the cations were detected during the INUIT-JFJ/CLACE 2013 campaign the grouping
24 of the clusters into different particle types by using certain marker peaks was difficult in some
25 cases. At the end, seven different particles types were extracted: black carbon (BC), organic
26 carbon (OC), internal mixture of black carbon and organic carbon (BC/OC), lead containing
27 particles, industrial metals, **Bio/Min/Sal** (containing possibly bioparticles, minerals or salts),
28 and minerals. The average mass spectra of each particle type are shown in Figure 1. The
29 association of the mass spectra to the individual particle types is explained in detail below.
30 The error limits of the number of mass spectra per particle types was estimated using counting
31 statistics.

32 *Organic fraction: Black carbon (BC) and organic carbon (OC)*

1 The clusters categorized as BC are due to the presence of the typical fragmentation of C_n^+
2 (Dall'Osto et al., 2004; Pratt and Prather, 2010) of higher mass-to-charge ratios (see Fig. 1a).
3 In comparison to the black carbon, the organic carbon cluster (Fig. 1b) shows different
4 fragmentations of aromatics ($[C_4H_3]^+$ (m/z 51); $[C_5H_3]^+$ (m/z 63); $[C_6H_5]^+$ (m/z 77); $[C_7H_7]^+$
5 (m/z 91) (Dall'Osto and Harrison, 2006; Pratt and Prather, 2010)), amines ($[CHN]^+$ (m/z 27);
6 $[C_3H_8N]^+$ (m/z 58) (Pratt and Prather, 2010)) or other organic material ($[C_2H_3]^+$ (m/z 27);
7 $[C_3H]^+$ (m/z 37); $[CH_3O/CHNO]^+$ (m/z 43); $[C_4H_2/C_3N]^+$ (m/z 50); $[C_3H_7O]^+$ (m/z 59);
8 $[C_{11}H_{10}/C_8H_{16}NO]^+$ (m/z 142) (Pratt and Prather, 2010)). Black carbon internally mixed with
9 organic (BC/OC) shows both fragmentation types of $[C_n]^+$ and $[C_nH_mNO]^+$ (Corbin et al.,
10 2012; Fig. 1c).

11 Closer consideration of the three different carbon clusters (BC, BC/OC, OC) shows that
12 potassium is present in nearly every mass spectrum in the background aerosol. In the
13 background aerosol 45282 mass spectra including black or organic carbon were measured:
14 92 % of all these mass spectra show potassium. The BC-type includes the mass spectra
15 without potassium (20 %; only 1 % in the OC/BC-type and 6 % in the OC-type). The same
16 observation holds for the IPR composition measured using the Ice-CVI (Section 3.1): The
17 particle types including organic carbon show more spectra including potassium (91 % of all
18 OC and OC/BC). In contrast to that the particle type including organic carbon measured while
19 using the ISI show more spectra without a high potassium peak (77 %). Previous
20 investigations show that the presence of high potassium peak in the mass spectra in
21 combination with organic carbon is a marker for biomass burning (e.g. Pratt and Prather,
22 2010; Twohy et al., 2010; Corbin et al., 2012) or biogenic aerosol (e.g. Trimborn et al., 2002;
23 Pratt and Prather, 2010). However, because only cations were measured during this
24 experiment, spectra with a potassium peak mixed with BC and OC cannot clearly assigned to
25 biomass burning or biological particles.

26 *Lead containing particles*

27 Previous measurements at the Jungfraujoch showed that lead-containing particles can be
28 found in IPR (Cziczo et al., 2009; Ebert et al., 2011). The cluster of lead containing particles
29 shows the typical isotope pattern of lead (m/z 208, 207, 206, 204; Fig. 1d).

30 *Industrial metals*

31 The cluster classified as 'industrial metals' (Fig. 1e) shows metal signals from anthropogenic
32 (urban/industrial) emissions like $[Cr]^+$ (m/z 52, 53, 54, 50), $[Co]^+$ (m/z 59), $[V]/[VO]^+$ (m/z

1 51/67), [Fe]⁺ (m/z 54, 56), [Mn]⁺ (m/z 55), [Ni]⁺ (m/z 58, 60, 61, 62) and [Zn]⁺ (m/z 64, 66,
2 68) (de Foy et al., 2012). Chromium and nickel containing particles might also be due to
3 contamination from stainless steel tubes. However, due to the low flow speed and laminar
4 flow conditions in our sampling tubes we can exclude abrasion of material by collision of
5 aerosol particles with the flow tube walls. Possible sources for steel contaminations particles
6 are only opening and closing of the valves. Thus, detection of such “industrial metals”
7 particles within a few seconds after opening/closing of a valve indicates contamination
8 artifacts. However, during these time periods no particles of the type “industrial metals” were
9 detected and therefore no particles were excluded as contamination.

10 *Bio/Min/Sal cluster*

11 The spectra in this cluster type contain only metal cations and can therefore not be
12 unambiguously be assigned to a certain particle type. The spectra in the *Bio/Min/Sal* cluster
13 show a mixture or single signals of [Na]⁺ (m/z 23), [Al]⁺ (m/z 27), [K]⁺ (m/z 39, 40), [Ca]⁺
14 (m/z 40) and/or [Fe]⁺ (m/z 54, 56). An example of an average spectrum of this particle type is
15 shown in Figure 1f.

16 The interpretation of this particle cluster is difficult. The signals are most likely cations of
17 different kinds of salts (K₂SO₄ or KNO₃ are more conceivable than sea salt), minerals or
18 primary biological particles, but without corresponding anion an unambiguously assignment
19 to one particle type is not possible. Previous investigations of biological aerosol have shown
20 that metal signals like [Na]⁺ (m/z 23), [K]⁺ (m/z 39) or [Ca]⁺ (m/z 40) dominate the cation
21 spectra (e.g. Frank et al., 2011; Pratt and Prather, 2010; Ferguson et al., 2004). During
22 laboratory studies with test aerosol we also observed mainly single metal signals of sodium
23 and potassium in biological particles, but as well in mineral dust particles. Also iron (Fe⁺ m/z
24 54, 56), which is a typical marker for mineral dust, was observed to occur in some biological
25 particles (maybe due to hemoglobin or due to other ions with an m/z of 56). For these reasons
26 the cluster “*Bio/Min/Sal*” cannot be further differentiated in this study.

27 *Minerals*

28 Typically marker peaks of minerals are: [Li]⁺ (m/z 6, 7), [Mg]⁺ (m/z 24, 25), [Al]⁺ (m/z 27),
29 [Si]/[SiO]⁺ (m/z 28, 29, 30/44), [Ca]⁺ (m/z 40), [Ti]/[TiO]⁺ (m/z 48, 46, 47, 49, 50/64) and/or
30 [Fe]⁺ (m/z 54, 56) (Trimborn et al., 2002; Dall’Osto et al., 2004; Dall’Osto et al., 2010)
31 Clusters containing at least three of the above marker peaks were classified as *minerals* (Fig.
32 1g).

1 *Others*

2 The cluster *others* includes all particle mass spectra, which are very noisy or could not be
3 unambiguously assigned to any of the above cluster types.

4

5 **3 Results and Discussion**

6 During the INUIT-JFJ/CLACE 2013 campaign we measured 71064 background aerosol
7 particles during a measurement time of 217 h and 1803 ice particle residuals during a
8 measurement time of 342 h: 1659 spectra behind the Ice-CVI during 273 h and 144 spectra
9 behind the ISI during 69 h.

10 **3.1 Ice particle residual composition and potential aerosol sources**

11 The ALABAMA was used to analyze ice crystals extracted from mixed-phase clouds by two
12 different inlets: ISI and Ice-CVI. The times during which cloud particles were sampled by the
13 ISI were identified using the cloud liquid water content (LWC)-data measured with two PVM
14 instruments (PSI and University of Manchester) and a CDP (University of Manchester) while
15 the times when the Ice-CVI sampled cloud particles were identified using the ice residual
16 concentration measured with the CPC behind the Ice-CVI. According to the Ice-CVI sampling
17 capability, which is described in section 2.3, the cloud event periods where the ALABAMA
18 was coupled to the Ice-CVI were classified. This classification resulted in (++)-sampling-
19 periods, when there was hardly any precipitation or blown snow, so that small secondary ice
20 particles created by crystal-crystal collisions can be neglected and thus INP containing
21 primary ice particles are sampled. For (+)-sampling-periods, the sampling of small secondary
22 ice particles, that do not contain a particle that served as INP, cannot be excluded, since
23 precipitation and blown snow occurred. As a consequence, the ice particle residues analyzed
24 during (++)-sampling-periods are attributed to INP whereas for (+)-sampling-periods this
25 relation is not that clear and might be only valid for particles that are larger than at least
26 300 nm. Table 1 shows the identified cloud events along with sampling time, number of
27 acquired mass spectra, sampling-period classification, and weather conditions and cloud type.
28 The meteorological situation during the whole campaign was mainly influenced by low
29 pressure systems with low temperatures.

30 The occurrence of artifacts during the measurements using the Ice-CVI as well as the ISI is
31 described in Worringer et al. (2015). Aluminum oxide is an artifact of the measurements with
32 the Ice-CVI and silicon oxide is an artifact of the measurements with the ISI. The impaction

1 plates of the Ice-CVI contain aluminum. When the ice crystals bounce on the impactation plates
2 of the Ice-CVI, some aluminum oxide particles are removed from these plates and can be
3 carried with the air stream to the analysis instrument. The ISI was calibrated with silicon
4 oxide particles, which are remained in the system and occurred during the measurements as
5 artifacts. In our dataset it is difficult to distinguish between artifacts and a real component of a
6 particle. Therefore the peaks of m/z 27 (Al^+) and m/z 43 (AlO^+) with respect of the Ice-CVI
7 measurements and the peak of m/z 28 (Si^+) with respect to the ISI measurements were
8 ignored.

9 ~~In total, we measured 329 spectra during the (++)-events (61 h measurement time) and 1335~~
10 ~~spectra during the (+)-events (160 h measurement time) by using the Ice-CVI. Behind the ISI~~
11 ~~we measured 144 spectra during 35 h measurement time.~~

12 Figure 2 shows the results of the clustering algorithm for all ice particle residual
13 measurements. The Ice-CVI data were analyzed separately for all (++)-sampling-periods (left
14 pie chart) and for all (+)-sampling-periods (middle pie chart). The right pie chart shows the
15 results for all ISI measurements. This analysis shows that the metal containing particle groups
16 (Bio/Min/Sal, industrial metals, and minerals) are the dominating fractions in IPR
17 composition measured by using the Ice-CVI during the (+)-sampling-periods (49 %) and the
18 ISI (66 %). Interestingly, during the (++)-sampling-periods metal containing particles
19 represent only a smaller fraction (40 %). We also detected lead containing particles, but only
20 while sampling through the Ice-CVI (7 % in the (++) cases and 12 % in the (+) cases).
21 During the (++)-sampling-periods measured behind the Ice-CVI, black carbon internally
22 mixed with organic carbon (20 %) is one of the main fractions. Together with OC (26 %),
23 these two particle types represent 46 % of all IPR. It is worth noting that there are more
24 similarities between the Ice-CVI and ISI during (+)-sampling-periods than the (++)-
25 sampling-periods. A reason for that can be that the ISI measurements are also influenced by
26 secondary ice or incoming snowflakes. During the (+)-sampling-periods as well as during the
27 ISI-sampling-periods precipitation occurred. On the other hand, the measurements at the ISI
28 and the Ice-CVI were not done simultaneously, such that also differences in the air mass
29 origin could play a role here.

30 Backward trajectories were compiled using CRISP (Klimach, 2012) with access to HYSPLIT
31 (Hybrid Single Particle Lagrangian Integrated Trajectory Model, National Oceanic and
32 Atmospheric Administration; Draxler and Rolph, 2012; Rolph, 2014), which was run using
33 GDAS (Global Data Assimilation System) meteorological dataset (starting altitude: 3580 m

1 asl.; hours back: 72 h; initialize time: end of the current event). The geographical origin of the
2 air masses and change of altitude during the transport can be used to infer whether the air
3 masses are influenced by surface emissions or mainly characterized by free tropospheric air
4 and long distance transport. During all measurement episodes (total, Ice-CVI, ISI) the air
5 masses approached the measurement station from slightly different directions (Fig. 3). The air
6 masses during the (++)-sampling-periods came primarily from north-western directions from
7 North America over France, while during the (+)-sampling-periods the air masses arrived
8 more from the North, over Scandinavia and Germany. The origin of the air masses during the
9 measurements using the ISI are similar to those of the (++)-sampling-periods but with a
10 tendency towards southern directions (Fig. 3). During non-cloud episodes air masses
11 approached the measurement location from all directions.

12 Previous measurements at the JFJ showed that there is an enrichment of mineral dust and
13 black carbon in IPR composition (Mertes et al., 2007; Cozic et al., 2008b; Kamphus et al.,
14 2010). An enrichment of black carbon is not observed in our measurements. Cziczo et al.
15 (2009) found that lead-containing particles are also enriched in the IPR compared to the
16 background aerosol. Our measurements show also that mineral dust (measured behind the ISI
17 and during the (+) sampling periods) and lead (only measured behind the Ice-CVI) were two
18 of the dominating fractions in the IPR composition. Worringen et al. (2015) report on SEM
19 analyses of particles sampled during the same project behind the ISI and the Ice-CVI. They
20 found lead in two states, namely homogeneous lead-rich particles and small lead inclusions in
21 particles of other material. While the small lead inclusions are not considered as potential
22 artifacts, the large lead-rich particles might be artifacts from mechanical re-suspension of lead
23 containing particles from the surface of the impaction plates of the Ice-CVI. In our case the
24 lead-containing particles are internally mixed with organics, minerals or other metals,
25 therefore we interpret these particles as real atmospheric particles and not as artifacts.

26

27 3.2 Event-to-event variability

28 Figure 4 shows the IPR chemical composition measured during seven different events. These
29 sampling-periods were chosen, because these are (++)-sampling-periods and contamination of
30 e.g. incoming snowflakes are excluded and during these sampling-periods the most particles
31 were measured (except for the ISI measurements). Although the air masses sampled during all
32 seven events have very similar origin and history of altitude (Fig. 5a and 5b) the chemical
33 composition for each event is different from the others. All air masses during these events

1 arrived rising from a western direction to the measurement platform, such that the chemical
2 composition of these seven events was probably influenced by local emissions. During Event
3 3 and 4 the air masses arrived from a south-western direction. This is reflected in the chemical
4 composition: Both events show organic carbon as the main fraction and the amount of lead
5 containing particles is comparable (13 % Event 3 and 15 % Event 4). The differences between
6 Event 3 and 4 are the absence of BC in Event 4 and of minerals in Event 3. The chemical
7 composition of Event 12 is also comparable to Event 4 and Event 6. In this case also the
8 dominating fractions are OC and Bio/Min/Sal. The absence of lead containing particles (as
9 well as in Event 6) and the presence of 2 % BC/OC in Event 12 or 4 % in Event 6 are the
10 main differences between Event 12, 6 and Event 4.

11 Another reason for similarities and differences between these 7 events can be the temperature
12 (Fig. 6). Events 3, 4 and 6 have the highest fraction of OC (nearly 50 % of the particles) and
13 Event 6 additionally a high amount of metal containing particles (37 %; industrial metals,
14 minerals and Bio/Min/Sal). Event 3 and 4 have also the highest temperatures (Event 3:
15 average temperature $\bar{T} = -7.8$ °C; Event 4: $\bar{T} = -8.6$ °C). In contrast to that, Event 12 has the
16 highest amount of metal containing particles (65 %) and has an average temperature of about
17 $\bar{T} = -17$ °C. Event 6 has also a high amount of metal containing particles and the lowest
18 average temperature of about $\bar{T} = -21$ °C. Event 4 has also a high amount (41 %) of 'metal'
19 components but by closer consideration of the Bio/Min/Sal-type it can be shown that this type
20 consists mostly of metal ions together with organic ions in Event 4 and more single metal ion
21 signals during Event 12 and 6. This high amount of metal components measured at lower
22 temperatures is also comparable to Event 2 and 5. 62 % of the chemical composition of Event
23 2 and 51 % of Event 5 consist of metal components. Therefore the data indicate that organic
24 material dominates the IPR composition at higher temperatures and metal components from
25 mineral or salty origin dominate at lower temperatures. This finding is surprising, because
26 previous studies found that organics are ice active only at temperatures below -40 °C (Hoose
27 and Möhler, 2012). However, the organic signal in the mass spectra might also originate from
28 bioparticles, which would explain the ice formation at higher temperatures, because
29 bioparticles have been reported in the literature by many authors to be ice active at higher
30 temperatures (e.g. Möhler et al., 2008; Hoose and Möhler, 2012). Another source can be soil
31 organic matter. Tobo et al. (2014) shows that organic-rich particles are more important than
32 mineral particles for the ice-nucleating ability of agricultural soil dust at temperatures higher
33 than -36 °C. An exception is Event 1. During this event the second lowest temperatures ($\bar{T} = -$
34 19.2 °C) of all events prevailed, but a high relative amount of organic components was

1 measured (80 % BC/OC and OC). A reason for this high relative amount of organic material
2 can be local emissions. At this time the total particle concentration (measured inside the cloud
3 using the total inlet) shows a short period with high concentrations ($> 2000 \text{ cm}^{-3}$, see Fig. 7),
4 which indicates local emissions.

6 3.3 Comparison between background aerosol particle composition and IPR

7 During non-cloud phases the ALABAMA was connected to the total inlet to measure
8 background aerosol particles. Figure 8 shows the averaged composition of all background
9 aerosol particles along with the IPR composition measured behind the Ice-CVI during the
10 (++)-sampling-periods and behind the ISI. The temperature range during the background
11 aerosol measurements was between $-27 \text{ }^{\circ}\text{C}$ and $-6 \text{ }^{\circ}\text{C}$, which is comparable to the temperature
12 range of the cloud events. In comparison to the IPR composition, the measurements show a
13 high fraction of black carbon (17 %; Fig. 8) and only a minor fraction of BC/OC (4 %). The
14 fraction of the particle type ‘BC/OC’ in the background aerosol is comparable to that in the
15 IPR sampled by the ISI. However, also the aerosol particles are dominated by the particle
16 types ‘organic carbon’ (43 %) and ‘Bio/Min/Sal’ (30 %). ~~Previous high mountain-top~~
17 ~~measurements at the Storm Peak Laboratory (SPL; 3200 m asl.) in northern Colorado show~~
18 ~~also organic as the major component in the background aerosol (DeMott et al., 2003a ;Cziczo~~
19 ~~et al., 2004a).~~ The differences as compared to the IPR compositions are the negligibly small
20 amount ($< 0.1 \text{ %}$) of lead-containing particles and the much smaller amount of minerals
21 (about 1 %). This is partly in contrast to other measurements. Previous measurements with the
22 ATOFMS at the Jungfrauoch as well as airborne measurements over North America show 5
23 and 10 % lead-containing particles in the background aerosol (Murphy et al., 2007) but also
24 only a small amount of mineral dust or fly ash measured at the Storm Peak Laboratory (SPL;
25 3200 m asl.) in northern Colorado (DeMott et al., 2003a). Data from the SPL show also
26 organic as the major component in the background aerosol (DeMott et al., 2003a ;Cziczo et
27 al., 2004a). A part of the organic material detected in the IPR as well as in the background
28 aerosol may be due to could be local anthropogenic emissions. In the vicinity of the
29 measurement station is a large and popular skiing region. Additionally, cooking emissions,
30 diesel exhaust or residential heating may also play a role.

~~Previous investigations show that the presence of a high potassium peak in the mass spectra in~~
32 ~~combination with organic carbon is a marker for biomass burning (e.g. Pratt and Prather,~~
33 ~~2010; Twohy et al., 2010; Corbin et al., 2012) or biogenic aerosol (e.g. Trimborn, 2002; Pratt~~
34 ~~and Prather, 2010). Closer consideration of the three different carbon clusters (BC, BC/OC,~~

1 OC) shows that potassium is present in nearly every mass spectrum. In the background
2 aerosol 45282 mass spectra including black or organic carbon were measured: 92 % of all
3 these mass spectra show potassium. The BC type includes the mass spectra without potassium
4 (20 %; only 1 % in the OC/BC type and 6 % in the OC type). The same observation holds for
5 the IPR composition: The particle types including organic carbon measured by the use of the
6 Ice-CVI as well as the ISI show more spectra including potassium (94 % of all OC and
7 OC/BC spectra while using the Ice-CVI and 98 % while using the ISI). Because of this results
8 spectra with a potassium peak cannot clearly assigned to biomass burning or biological
9 particles.

11 3.4 Influence of the air mass trajectories on the aerosol composition

12 The chemical composition of the background (out-of-cloud) aerosol has been shown in Figure
13 8. The high variability of the measured IPR might be due to the different aerosol properties
14 when air masses arrive from different geographic origin and/or different altitudes at the
15 Jungfrauoch. Therefore, we investigate here how air masses origin influences the aerosol
16 properties. Because of the saddle position of the JFJ, there are only two possibilities of how
17 the air masses can approach the measurement platform (Fig. 6). Predominantly, the air masses
18 arrive from northwestern direction over the Swiss plateau (wind direction of approx. 315°).
19 Less frequently, the approach was from a southeastern direction from the inner Alps (approx.
20 135°, via the Aletsch Glacier). According to the direction from which air masses approach the
21 measurement platform, the chemical composition is influenced predominantly by
22 anthropogenic and organic emissions or by mineral dust sources. To assess the influence of
23 origin and the average altitude of the air masses during their transport to the Jungfrauoch, we
24 compare two time periods with aerosol measurements using the total inlet (11.02. and
25 19.02.2013). The chosen time periods exhibit nearly the same relative humidity, potential wet
26 bulb temperature and temperature (Fig. 6).

27 Fig. 9 shows the chemical composition of the aerosol particles for both time periods, along
28 with corresponding back-trajectories. The comparison shows that more particles containing
29 BC (internally mixed with ammonium or the Bio/Min/Sal-type) and the Bio/Min/Sal-type are
30 observed in the air masses arriving from a northwestern direction (11.02.2013), while the
31 measurements during the SE-event show more OC containing particles (internally mixed with

1 ammonium or the Bio/Min/Sal-type). The fraction of particles measured containing only
2 potassium and pure organic carbon is very similar for both events.

3 The air masses not only approached locally from different directions, but also had different
4 long-range origins (see back trajectories Fig. 9). The air masses measured on 19.02.2013
5 (NW-event) approached from the north over Germany and have remained at approximately
6 the same altitude as the Jungfrauoch during the last 72 hours. Thus, these air masses have
7 been in the free troposphere for at least three days prior to the measurement. The chemical
8 composition of the measured particles is dominated by black carbon internally mixed with
9 ammonium and by the Bio/Min/Sal-type. In contrast to the 19.02.2013, the air masses on
10 11.02.2013 (SE-event) approached over southern France and the western Po Valley, have
11 been lifted from low altitudes and clearly influenced by the boundary layer. These air masses
12 contain higher amounts of OC containing particles. This shows that the vertical uplifting
13 brings anthropogenic emissions (e.g., from the Po Valley) up to the altitude of the
14 measurement station, while the air masses measured during the NW-event contain a higher
15 amount of sea salt or mineral dust (both contained in the Bio/Min/Sal-type) and aged,
16 processed BC particles.

17

18 3.5 Size distribution of IPR and background aerosol

19 Ice-CVI and ISI both extract small ice particles in the size range from 5 μm to 20 μm from
20 mixed-phase clouds (Mertes et al., 2007; Kupiszewski et al., 2014) while the upper cut-off of
21 the total inlet was 40 μm for wind speeds up to 20 m/s (Weingartner et al., 1999). In Figure 10
22 is shown the size distributions of IPR measured with the ALABAMA (a, c, e) and the Sky-
23 OPC (b, d, f) compared with ESEM measurements (a and b). Figure 10a shows the size
24 distributions of IPR measured by ALABAMA and ESEM applying the Ice-CVI. Figure 10e
25 the size distributions measured by ALABAMA and ESEM using the ISI. In Figure 10b and d,
26 the corresponding size distributions measured with the Sky-OPC are shown. Figure 10c
27 shows the size distributions measured by ALABAMA and Fig. 10d measured by the Sky-
28 OPC using the ISI. Fig. 10e and f show the size distribution measured by ALABAMA and the
29 Sky-OPC using the total inlet. The measurement times for Ice-CVI and ISI are given in Table
30 1; the measurements using the total inlet were done during all cloud-free periods. For all three
31 inlets (total, Ice-CVI, ISI) most of the detected IPR measured with the ALABAMA and also
32 with the Sky-OPC is in the size range of 300–650 nm. The IPR size distributions measured
33 by ALABAMA and SEM behind the Ice-CVI are in very good agreement (Fig. 10a). In

1 contrast, the IPR size distribution measured behind the ISI are somewhat different. (Fig. 10c):
2 Both distributions show two maxima, but the positions of the maxima are not the same. The
3 ALABAMA IPR distribution has a primary maximum in the size bin 0.4–0.5 μm and a
4 secondary maximum in the size bin 1.3–1.6 μm . The SEM IPR distribution both maxima are
5 shifted to larger sizes. The first maximum is in the 1–1.5 μm interval and the second
6 maximum is in the 2–2.5 μm interval. However, total count rates are very low, so this
7 difference should not be overemphasized. Furthermore, SEM measured geometric diameters,
8 while the sizes determined by ALABAMA refer to the vacuum aerodynamic diameter. SEM
9 and ALABAMA measure the size distribution in different ways: ALABAMA measures
10 vacuum aerodynamic diameter and SEM geometric diameter. To compare both data sets the
11 SEM data were converted to the aerodynamic diameter. The vacuum aerodynamic diameter
12 was calculated according to DeCarlo et al. (2004) with the assumption that the projected area
13 diameter from the electron microscopy analysis equals the volume-equivalent diameter.
14 Furthermore, an average dynamic shape factor of 1.2 was used for the calculations. This
15 seems to be justified, as most non-extremely shaped particles show low variation in shape
16 factor (Schneider et al., 2006; Zelenyuk et al., 2006), except for soot with high fractal
17 dimension (Slowik et al., 2004) which was not commonly encountered in the present work.
18 The density ratios required for the calculation were estimated from the major composition of
19 the particle according to the values from Weinbruch et al. (2014) (Table S2). The IPR size
20 distributions measured by ALABAMA and SEM behind the Ice-CVI show the same behavior
21 (Fig. 10a) with shifting the SEM graph to larger sizes. Both distributions show a slow
22 increase at small size ranges and a higher number of larger particles. The ALABAMA IPR
23 distribution has a primary maximum in the size bin 300–400 μm and a secondary maximum
24 in the size bin 500–600 μm . The SEM size distribution shows a single maximum at about
25 900 μm . However, total count rates are very low, so this difference should not be
26 overemphasized. For all three inlets (total, Ice-CVI, ISI) most of the detected particles
27 measured with the ALABAMA are in the size range of 300–800 nm. In contrast to the size
28 distribution measured with the ALABAMA (and also ESEM for the Ice-CVI), the size
29 distributions measured with Sky-OPC (b, d, f) do not show a maximum but only a decreasing
30 number concentration of particles with increasing particle diameter for all three inlet types.
31 The difference to the ALABAMA size distributions is a result of the detection and ionization
32 efficiency of the ALABAMA which is the highest around 400 nm. The IPR size distributions
33 measured with the ESEM and Sky-OPC (10b) show both a decreasing number of particles at
34 larger size ranges. In contrast to the size distribution measured with the Sky-OPC the size

1 distribution measured with ESEM shows a lower number of particles at smaller size ranges.
2 The Sky-OPC size distribution measured behind the ISI (10d) shows an unexplained sudden
3 decrease above 3 μm . Figure 10f shows that the background aerosol particles (Sky-OPC) have
4 a size range of up to approximately 20 μm but with highest number concentration in the
5 smaller range ($< 1 \mu\text{m}$). The relative amount of larger particles is ($d > 1 \mu\text{m}$) clearly elevated
6 for the IPR, both behind the ISI and Ice-CVI (10b and d) in comparison to the background
7 particles (10f). Note that the measurements of background particles (out of cloud) and IPR
8 were conducted by definition at different times, such that the absolute amount of particles
9 cannot be compared.

10 As mentioned above, relatively more IPR larger than 1 μm were observed compared to the
11 background aerosol particles. The percentage of the background aerosol particles larger than
12 1 μm (vacuum aerodynamic diameter) measured by ALABAMA was only 3 %, while 12 -
13 13 % of the IPR behind the Ice-CVI and ISI were larger than 1 μm . Therefore, the chemical
14 composition of these particles has been analyzed separately:

15 Figure 11 shows the chemical composition of the IPR and background aerosol particles larger
16 than 1 μm . The most frequent particle types found in the IPR larger than 1 μm are OC, lead
17 containing particles, Bio/Min/Sal, and minerals for the Ice-CVI, and Bio/Min/Sal and
18 minerals for the ISI. Lead containing particles are found in the IPR sampled by the Ice-CVI to
19 a similar percentage (14 %) as in all IPR (7 %, see Figs. 2 and 8). Interestingly, the
20 background aerosol supermicron particles are dominated by the Bio/Min/Sal-type and OC.
21 The finding strengthens the assumption that the metal ions detected in these mass spectra are
22 likely metal cations of primary aerosol like sea salt, minerals or biological particles, which are
23 mainly found in the coarse mode (e.g., Seinfeld and Pandis, 2006). Such large primary
24 particles are also expected to act efficiently as INP, and it is therefore not surprising that they
25 are found in the supermicrom IPR. More surprising is the large fraction of OC and BC/OC
26 particles detected in the supermicron IPR. These large particles containing organic material
27 appear to be even better INP than the supermicron particles assigned to the Bio/Min/Sal
28 category. It has recently been suggested that porous and glassy organic particles under certain
29 conditions play an important role as INP (Murray et al., 2010; Adler et al., 2013), and this
30 may explain the results presented here. But also the origin of these supermicron organic
31 particles remains unclear. Primary biological material as a source for these particles is
32 regarded to be unlikely, because the marker peaks observed in cations of biological particles
33 (like K^+ , Na^+ , Ca^{2+}) were not observed in these particle spectra assigned to the OC and BC/OC

1 types. However, particle classification of single particle mass spectra is never absolutely
2 certain, and future work may reveal more insight into the nature and origin of these particles.

3 The particle composition of the particle smaller than 1000 nm closely resembled the
4 composition of the whole data set, because the particle smaller than 1000 nm dominate the
5 analyzed particles by number. Only the BC/OC-type is increased in the particles smaller than
6 1000 nm measured while using the Ice-CVI.

7 The size distribution allow also for an estimation of the ice active site (e.g., Vali et al., 2014)
8 density of particles larger than 1 μm compared to those smaller than 1 μm : Assuming that
9 each IPR corresponds to at least one ice active site on the original aerosol particle (otherwise
10 it would not have acted as an INP), we can estimate the ice active site density for the particles
11 analyzed by ALABAMA, separated for particles smaller than 1 μm and larger than 1 μm . The
12 number of ice active sites per IPR surface (ice active site density) is $2.0 \cdot 10^{-7} \text{ nm}^{-2}$ for
13 $d > 1 \mu\text{m}$ and $1.6 \cdot 10^{-6} \text{ nm}^{-2}$ for particles with $d < 1 \mu\text{m}$. Relating the number of ice active sites
14 to the total aerosol surface yields $7.1 \cdot 10^{-10} \text{ nm}^{-2}$ for $d > 1 \mu\text{m}$ and $4.3 \cdot 10^{-9} \text{ nm}^{-2}$ for $d < 1 \mu\text{m}$.
15 In both cases the ice active site density is larger for particles smaller than 1 μm . This is an
16 important finding and explains the high number of IPR found in the size range below 1 μm .
17 However, it should be noted that the assumption that each IPR corresponds to one ice active
18 site may underestimate the number of ice active sites. In cases where more than one ice active
19 site is found on the particles, also only one ice crystal will form and one IPR will remain.
20 Thus the estimated number yields a lower limit for the ice active sites.

22 4 Summary and Conclusions

23 This paper presents results of the single particle measurements during the INUIT-JFJ/CLACE
24 2013 campaign conducted at the Jungfraujoch in January/February 2013. In agreement with
25 previous measurements at the Jungfraujoch (Chou et al., 2011; Kamphus et al., 2010; Mertes
26 et al., 2007), it was found that larger particles are more efficient ice nuclei. Specific analysis
27 of only those particles $> 1 \mu\text{m}$ showed that the chemical composition of these larger particles
28 is dominated by organic material and the "Bio/Min/Sal" type, both in the IPR as well as in the
29 background aerosol. Besides, the "minerals" group was found to be one of the main fractions
30 of the IPR measured behind the Ice-CVI. From the finding that IPR have a higher relative
31 number of larger particles than the background aerosol particles we conclude and confirm a
32 better ice nucleation ability for the larger, primary aerosol particles such as minerals, salt and
33 biological particles.

1 In general, IPR are enriched in organic material, partly also internally mixed with BC.
2 Additionally, minerals and lead were found in IPR as has already been observed in previous
3 measurements conducted at the JFJ (Mertes et al., 2007; Cozic et al., 2008b; Cziczo et al.,
4 2009; Kamphus et al., 2010; Ebert et al., 2011). In comparison to the composition of the IPR
5 measured using the Ice-CVI, the measured composition using the ISI is dominated by
6 minerals, and no lead containing particles were found, while 7 % of the IPR sampled using
7 the Ice-CVI included lead. In contrast to Cozic et al. (2008) we found no enrichment of pure
8 black carbon in the IPR composition. Only the chemical composition of the background
9 aerosol particles shows a high fraction of black carbon. These results agree with previous
10 investigations (DeMott et al., 1999; Dymarska et al., 2006; Hoose and Möhler, 2012)
11 describing black carbon as a good ice nucleus but only at lower temperatures and its ice
12 nucleating ability appears to be reduced if coatings by organic material or sulfuric acid are
13 present. During the INUIT-JFJ/CLACE 2013 campaign the temperatures were never lower
14 than -30 °C; see Fig. 6. In the background aerosol, the main particle fraction is also organic
15 carbon. The high amount of organic material in the background aerosol as well as in the IPR
16 motivates further investigation of different organic material by single particle mass
17 spectrometry to better characterize the organic fraction. While there have been previous
18 observations that organic matter is of general importance for ice nucleation ability (DeMott et
19 al., 2003a; Cziczo et al., 2004b), recent laboratory studies have shown the importance of
20 porous and glassy organic matter for ice nucleation (Murray et al., 2010; Adler et al., 2013).
21 The investigation of the influence of the temperature and the origin and altitude of the air
22 masses on the chemical composition of IPR and aerosol particles indicate that organic
23 material dominates the IPR composition at higher temperatures and metal components from
24 mineral or salt at lower temperatures which agrees with previous findings (e.g. Möhler et al.,
25 2008; Hoose and Möhler, 2012). It was illustrated that the origin (geographic and altitude) of
26 the air masses influenced the chemical composition of the aerosol particles. For the non-cloud
27 aerosol, the particles sampled in air masses characterized by free tropospheric air and long
28 distance transport were found to be dominated by BC and single metal ions from salt, mineral
29 or biological sources (Bio/Min/Sal-type). These particle types were probably partly mixed
30 with secondary inorganic components, because NH_4^+ was detected in some spectra. In contrast
31 to that, the particles in air masses which are influenced by surface emissions are dominated by
32 organic carbon and potassium.

33

34 **Appendix A: Parameters underlying the clustering algorithm**

1 This section describes the cluster parameters of the software package CRISP. The chosen
2 parameters are listed in Table A.

3 *Normalization type and time*

4 To compensate for differences in the ionization efficiency, each mass spectrum is normalized
5 to the sum of the signal intensities with preservation of the relative relationship of the signals.
6 By this, the influence of absolute signal intensity is decreased. Absolute signal intensity is not
7 needed because the laser ablation method does not measure quantitatively. The point at which
8 the normalization is applied in the analysis sequence can be chosen. In case of measuring both
9 polarities the spectra of both polarities are first merged, and normalization can be applied
10 before, after or before and after concatenation.

11

12 *Preprocessing type*

13 Preprocessing (before normalization) can be applied to increase mass signals with lower
14 intensity with respect to signals with a higher intensity, such that the presence of a certain m/z
15 has more significance than the signal intensity in the calculation of the distance to the
16 reference spectrum. Typically the square root of the signal intensities is used.

17

18 *Initialisation type*

19 This parameter defines the way the reference mass spectra are selected. Two options are
20 available:

- 21 - *find different startcluster*: different spectra are randomly selected according to certain
22 criteria
- 23 - *random*: reference spectra are chosen randomly

24 Reference spectra can also be determined manually, however, this last option is not very
25 useful for field data because the number of particle types is unknown.

26

27 *Number of cluster*

28 The result of the clustering is highly dependent on the pre-selected number of clusters. In the
29 case that the number of clusters is too small, some cluster types cannot be found, while in the
30 case that the number is too large, too many similar spectra are assigned to different clusters.
31 In the fuzzy c-means algorithm all non-matched spectra are collected in a rest cluster.

32

33 *Cluster difference*

1 This parameter determines the distance between the spectra which are chosen as start
 2 references at 'find different startcluster'. The *cluster difference* is between 1 and 0, where a
 3 *cluster difference* of 1 means that the chosen startclusters are identically. This distance results
 4 from the Pearson correlation and affects the number of the resulting clusters. The number of
 5 clusters increases with increasing similarity of the references and is constant at a value of 0.7
 6 (Roth, 2014). If the *cluster difference* is too small, the distinctions between the clusters are too
 7 large, resulting in too few cluster types. Thus, it is recommended to use more similar
 8 reference mass spectra and to summarize those clusters that show similar mass spectra at the
 9 end of the clustering.

10

11 *Fuzzifier and fuzzy abort*

12 The *fuzzifier* (also called *fuzzy weighting* exponent) is a dimension of fuzziness of the
 13 classification of the cluster ($1 \leq \textit{fuzzifier} \leq \infty$; e.g. Huang et al., 2012). The bigger the
 14 *fuzzifier*, the more inaccurate is the assignment to the references, because the spectra cannot
 15 exactly be assigned to one cluster. The distance d_{ij} between spectra i and reference j is
 16 weighted with:

$$17 \quad d_{ij}^{\frac{1}{z-1}} \quad (1)$$

18 where z is the *fuzzifier*. When the preprocessing option of CRISP is used, it has been found
 19 that the result of the clustering is independent of the *fuzzifier* value (Roth, 2014).

20 During the clustering, each mass spectrum is compared to the reference spectra in terms of
 21 distance, membership and correlation. If these parameters fulfill the pre-selected criteria, the
 22 mass spectrum is sorted into the cluster represented by the reference and the average spectrum
 23 is calculated again. Subsequently all mass spectra are compared again with the reference
 24 spectra. This procedure is repeated until the criterion of abort (*fuzzy abort*) is reached, such
 25 that the clustering stops when the value of the difference of all reference spectra between two
 26 iterations is smaller than the value defined by *fuzzy abort*.

27 For the data evaluation of the current dataset (both IPR and background aerosol particles) a
 28 mixture of manual and automatic clustering was used. First, an automatic clustering was done
 29 with the following parameters:

30

31 Table A: Chosen clustering parameter.

Preprocessing type	Power each m/z
Preprocessing power	0.5
Normalization type	Sum
Cluster difference	0.7 (0.6)
Distance	Correlation
Fuzzifier	1.2
Fuzzy abort	0.0001

1
2 As already mentioned the result of the clustering is highly dependent on the chosen initial
3 number of clusters. If this initial number of clusters is too small, some cluster types may not
4 be found. Therefore we chose a high number of clusters. In the case of the background aerosol
5 (71064 spectra) we started the first clustering with 200 clusters. Each of the resulting 200
6 clusters was manually inspected, and based on its ion signatures it was assigned to one
7 particle type. Those spectra that cannot be sorted by the algorithm into one of the 200 clusters
8 (membership coefficient below a pre-defined threshold) are assigned to a “rest cluster”
9 (12407 spectra in the case of the background aerosol). This rest cluster was clustered again
10 with a reduced condition for the cluster difference and with an initial number of clusters of 25.
11 The number of cluster was still too large after the clustering of the “rest cluster”, so it was
12 further analyzed. First, the remaining spectra were sorted by the use of specific marker peaks
13 and the resulting clusters were then clustered again with changing the fuzzifier from 1.2 to
14 1.3 and a cluster difference of 0.7. After that, the resulting clusters were manually inspected
15 and sorted (with the criterion $r^2 \geq 0.7$). By this, we could reduce the number of spectra in the
16 rest cluster from 12407 to 3243. Due to this sorting procedure based on both automatic
17 clustering and manual cluster inspection one particle type typically contains different clusters
18 with different fragmentations. For example, the particle type “organic carbon” includes
19 clusters showing aliphatic hydrocarbon, aromatic carbon, nitrogen and oxidized carbon
20 fragmentation patterns. In order to restrict the result to a reasonable number of particle types,
21 we summarized these clusters to one particle type.

22

23 Acknowledgements

24 This work was supported by the DFG projects FOR 1525 (INUIT), SPP 1294 (HALO, grant
25 Me 3524/1-2), the Max Planck Society, the European Union Seventh Framework Programme

1 (FP7/2007-2013) under grant agreement n° 2662254 (ACTRIS TNA) and the Swiss National
2 Science Foundation (200021L 135356).

3 The authors gratefully acknowledge the NOAA Air Resources Laboratory (ARL) for the
4 provision of the HYSPLIT transport and dispersion model and/or READY website
5 (<http://www.ready.noaa.gov>) used in this publication.

6

7 We would like to thank Swiss Meteorological Institute (MeteoSwiss) for providing
8 meteorological measurements and the International Foundation High Altitude Research
9 Station Jungfraujoch and Gornergrat (HFSJG) for the opportunity to perform experiments at
10 the Jungfraujoch. Additional thanks go to Oliver Appel (MPIC Mainz) for help with OPC
11 error calculations, to Oliver Schlenczek (University Mainz) for cloud observations at the JFJ
12 and to Udo Kästner (TROPOS) for his help during the measurements at the JFJ.

13

1 **References**

- 2 Abbatt, J. P., Benz, S., Cziczo, D. J., Kanji, Z., Lohmann, U., and Möhler, O.: Solid
3 ammonium sulfate aerosols as ice nuclei: a pathway for cirrus cloud formation, *Science*, 313,
4 1770-1773, 2006.
- 5 Adler, G., Koop, T., Haspel, C., Taraniuk, I., Moise, T., Koren, I., Heiblum, R. H., and
6 Rudich, Y.: Formation of highly porous aerosol particles by atmospheric freeze-drying in ice
7 clouds, *Proceedings of the National Academy of Sciences of the United States of America*,
8 110, 20414-20419, 2013.
- 9 Atkinson, J. D., Murray, B. J., Woodhouse, M. T., Whale, T. F., Baustian, K. J., Carslaw, K.
10 S., Dobbie, S., O'Sullivan, D., and Malkin, T. L.: The importance of feldspar for ice
11 nucleation by mineral dust in mixed-phase clouds, *Nature*, 498, 355-358, 2013.
- 12 Bezdek, J. C., Ehrlich, R., and Full, W.: Fcm - the Fuzzy C-Means Clustering-Algorithm,
13 *Computers & Geosciences*, 10, 191-203, 1984.
- 14 Brands, M., Kamphus, M., Böttger, T., Schneider, J., Drewnick, F., Roth, A., Curtius, J.,
15 Voigt, C., Borbon, A., Beekmann, M., Bourdon, A., Perrin, T., and Borrmann, S.:
16 Characterization of a Newly Developed Aircraft-Based Laser Ablation Aerosol Mass
17 Spectrometer (ALABAMA) and First Field Deployment in Urban Pollution Plumes over Paris
18 During MEGAPOLI 2009, *Aerosol Science and Technology*, 45, 46-64, 2011.
- 19 Cantrell, W., and Heymsfield, A.: Production of Ice in Tropospheric Clouds: A Review, in:
20 *Bulletin of the American Meteorological Society*, 6, 795-807, 2005.
- 21 Chen, Y., Kreidenweis, S. M., McInnes, L. M., Rogers, D. C., and DeMott, P. J.: Single
22 particle analyses of ice nucleating aerosols in the upper troposphere and lower stratosphere,
23 *Geophysical Research Letters*, 25, 1391-1394, 1998.
- 24 Chou, C., Stetzer, O., Weingartner, E., Jurányi, Z., Kanji, Z. A., and Lohmann, U.: Ice nuclei
25 properties within a Saharan dust event at the Jungfraujoch in the Swiss Alps, *Atmospheric
26 Chemistry and Physics*, 11, 4725-4738, 2011.
- 27 Corbin, J. C., Rehbein, P. J. G., Evans, G. J., and Abbatt, J. P. D.: Combustion particles as ice
28 nuclei in an urban environment: Evidence from single-particle mass spectrometry,
29 *Atmospheric Environment*, 51, 286-292, 2012.
- 30 Cozic, J., Mertes, S., Verheggen, B., Cziczo, D. J., Gallavardin, S. J., Walter, S.,
31 Baltensperger, U., and Weingartner, E.: Black carbon enrichment in atmospheric ice particle
32 residuals observed in lower tropospheric mixed phase clouds, *Journal of Geophysical
33 Research-Atmospheres*, 113, D15209, 2008a.
- 34 Cozic, J., Verheggen, B., Weingartner, E., Crosier, J., Bower, K. N., Flynn, M., Coe, H.,
35 Henning, S., Steinbacher, M., Henne, S., Collaud Coen, M., Petzold, A., and Baltensperger,
36 U.: Chemical composition of free tropospheric aerosol for PM1 and coarse mode at high
37 alpine site Jungfraujoch, *Atmospheric Chemistry and Physics*, 8, 407-423, 2008b.
- 38 Cziczo, D. J., DeMott, P. J., Brock, C., Hudson, P. K., Jesse, B., Kreidenweis, S. M., Prenni,
39 A. J., Schreiner, J., Thomson, D. S., and Murphy, D. M.: A Method for Single Particle Mass
40 Spectrometry of Ice Nuclei, *Aerosol Science and Technology*, 37, 460-470, 2003.
- 41 Cziczo, D. J., DeMott, P. J., Brooks, S. D., Prenni, A. J., Thomson, D. S., Baumgardner, D.,
42 Wilson, J. C., Kreidenweis, S. M., and Murphy, D. M.: Observations of organic species and
43 atmospheric ice formation, *Geophysical Research Letters*, 31, L12116, 2004a.

- 1 Cziczo, D. J., Murphy, D. M., Hudson, P. K., and Thomson, D. S.: Single particle
2 measurements of the chemical composition of cirrus ice residue during CRYSTAL-FACE,
3 *Journal of Geophysical Research-Atmospheres*, 109, D04201, 2004b.
- 4 Cziczo, D. J., Stetzer, O., Worrigen, A., Ebert, M., Weinbruch, S., Kamphus, M.,
5 Gallavardin, S. J., Curtius, J., Borrmann, S., Froyd, K. D., Mertes, S., Möhler, O., and
6 Lohmann, U.: Inadvertent climate modification due to anthropogenic lead, *Nature*
7 *Geoscience*, 2, 333-336, 2009.
- 8 Dall'Osto, M., Beddows, D. C. S., Kinnersley, R. P., and Harrison, R. M.: Characterization of
9 individual airborne particles by using aerosol time-of-flight mass spectrometry at Mace Head,
10 Ireland, *Journal of Geophysical Research*, 109, D21302, 2004.
- 11 Dall'Osto, M., and Harrison, R. M.: Chemical characterisation of single airborne particles in
12 Athens (Greece) by ATOFMS, *Atmospheric Environment*, 40, 7614-7631, 2006.
- 13 Dall'Osto, M., Harrison, R. M., Highwood, E. J., O'Dowd, C., Ceburnis, D., Querol, X., and
14 Achterberg, E. P.: Variation of the mixing state of Saharan dust particles with atmospheric
15 transport, *Atmospheric Environment*, 44, 3135-3146, 2010.
- 16 de Foy, B., Smyth, A. M., Thompson, S. L., Gross, D. S., Olson, M. R., Sager, N., and
17 Schauer, J. J.: Sources of nickel, vanadium and black carbon in aerosols in Milwaukee,
18 *Atmospheric Environment*, 59, 294-301, 2012.
- 19 DeCarlo, P. F., Slowik, J. G., Worsnop, D. R., Davidovits, P., and Jimenez, J. L.: Particle
20 Morphology and Density Characterization by Combined Mobility and Aerodynamic Diameter
21 Measurements. Part 1: Theory, *Aerosol Science and Technology*, 38, 1185-1205, 2004.
- 22 DeMott, P. J., Rogers, D. C., Kreidenweis, S. M., Chen, Y., Twohy, C. H., Baumgardner, D.,
23 Heymsfield, A. J., and Chan, K. R.: The role of heterogeneous freezing nucleation in upper
24 tropospheric clouds: Inferences from SUCCESS, *Geophysical Research Letters*, 25, 1387-
25 1390, 1998.
- 26 DeMott, P. J., Chen, Y., Kreidenweis, S. M., Rogers, D. C., and Sherman, D. E.: Ice
27 formation by black carbon particles, *Geophysical Research Letters*, 26, 2429-2432, 1999.
- 28 DeMott, P. J., Cziczo, D. J., Prenni, A. J., Murphy, D. M., Kreidenweis, S. M., Thomson, D.
29 S., Borys, R., and Rogers, D. C.: Measurements of the concentration and composition of
30 nuclei for cirrus formation, *Proceedings of the National Academy of Sciences of the United*
31 *States of America*, 100, 14655-14660, 2003a.
- 32 DeMott, P. J., Sassen, K., Poellot, M. R., Baumgardner, D., Rogers, D. C., Brooks, S. D.,
33 Prenni, A. J., and Kreidenweis, S. M.: African dust aerosols as atmospheric ice nuclei,
34 *Geophysical Research Letters*, 30, 10.1029/2003gl017410, 2003b.
- 35 DeMott, P. J., Prenni, A. J., Liu, X., Kreidenweis, S. M., Petters, M. D., Twohy, C. H.,
36 Richardson, M. S., Eidhammer, T., and Rogers, D. C.: Predicting global atmospheric nuclei
37 distributions and their impacts on climate, *Proceedings of the National Academy of Sciences*
38 *of the United States of America*, 107, 11217-11222, 2010.
- 39 Diehl, K., Quick, C., Matthias-Maser, S., Mitra, S. K., and Jaenicke, R.: The ice nucleating
40 ability of pollen - Part I: Laboratory studies in deposition and condensation freezing mode,
41 *Atmospheric Research*, 58, 75-87, 2001.
- 42 Diehl, K., and Wurzler, S.: Air parcel model simulations of a convective cloud: Bacteria
43 acting as immersion ice nuclei, *Atmospheric Environment*, 44, 4622-4628, 2010.
- 44 Diehl, K., Debertshäuser, M., Eppers, O., Schmithüsen, H., Mitra, S. K., and Borrmann, S.:
45 Particle surface area dependence of mineral dust in immersion freezing mode: investigations

1 with freely suspended drops in an acoustic levitator and a vertical wind tunnel, Atmospheric
2 Chemistry and Physics 14, 12343-12355, 2014.

3 Draxler, R. R., and Rolph, G. D.: HYSPLIT (HYbrid Single-Particle Lagrangian Integrated
4 Trajectory) Model access via NOAA ARL READY Website
5 (<http://ready.arl.noaa.gov/HYSPLIT.php>), NOAA Air Resources Laboratory, Silver Spring,
6 MD, 2012.

7 Dymarska, M., Murray, B. J., Sun, L., Eastwood, M. L., Knopf, D. A., and Bertram, A. K.:
8 Deposition ice nucleation on soot at temperatures relevant for the lower troposphere, Journal
9 of Geophysical Research-Atmospheres, 111, D04204, 2006.

10 Ebert, M., Worringer, A., Benker, N., Mertes, S., Weingartner, E., and Weinbruch, S.:
11 Chemical composition and mixing-state of ice residuals sampled within mixed phase clouds,
12 Atmospheric Chemistry and Physics, 11, 2805-2816, 2011.

13 Fergenson, D. P., Pitesky, M. E., Tobias, H. J., Steele, P. T., Czerwieniec, G. A., Russell, S.
14 C., Lebrilla, C. B., Horn, J. M., Coffee, K. R., Srivastava, A., Pillai, S. P., Shih, M.-T. P.,
15 Hall, H. L., Ramponi, A. J., Chang, J. T., Langlois, R. G., Estacio, P. L., Hadley, R. T., Frank,
16 M., and Gard, E. E.: Reagentless Detection and Classification of Individual Bioaerosol
17 Particles in Seconds, Analytic Chemistry, 76, 373-378, 2004.

18 Frank, M., Gard, E. E., Tobias, H. J., Adams, K. L., Bogan, M. J., Coffee, K. R., Farquar, G.
19 R., Fergenson, D. P., Martin, S. I., Pitesky, M., Riot, V. J., Srivastava, A., Steele, P. T., and
20 Williams, A. M.: Single-Particle Aerosol Mass Spectrometry (SPAMS) for High-Throughput
21 and Rapid Analysis of Biological Aerosols and Single Cells, in: Rapid Characterization of
22 Microorganisms by Mass Spectrometry, American Chemical Society, Washington, DC, 161-
23 196, 2011.

24 Froyd, K. D., Murphy, D. M., Lawson, P., Baumgardner, D., and Herman, R. L.: Aerosols
25 that form subvisible cirrus at the tropical tropopause, Atmospheric Chemistry and Physics, 10,
26 209-218, 2010.

27 Fukuta, N., and Takahashi, T.: The Growth of Atmospheric Ice Crystals: A Summary of
28 Findings in Vertical Supercooled Cloud Tunnel Studies, Journal of the Atmospheric Sciences,
29 56, 1963-1979, 1999.

30 Gerber, H.: Microphysics of Marine Stratocumulus Clouds with Two Drizzle Modes, Journal
31 of the Atmospheric Sciences, 53, 1649-1662, 1996.

32 Hartmann, S., Niedermeier, D., Voigtländer, J., Clauss, T., Shaw, R. A., Wex, H., Kiselev, A.,
33 and Stratmann, F.: Homogeneous and heterogeneous ice nucleation at LACIS: operating
34 principle and theoretical studies, Atmospheric Chemistry and Physics, 11, 1753-1767, 2011.

35 Heim, M., Mullins, B. J., Umhauer, H., and Kasper, G.: Performance evaluation of three
36 optical 30 particle counters with an efficient "multimodal" calibration method, Journal of
37 Aerosol Science, 39, 1019-1031, 2008.

38 Hinz, K.-P., Greweling, M., Drews, F., and Spengler, B.: Data Processing in On-line Laser
39 Mass Spectrometry of Inorganic, Organic, or Biological Airborne Particles, American Society
40 for Mass Spectrometry, 10, 648-660, 1999.

41 Hoose, C., Kristjánsson, J. E., and Burrows, S. M.: How important is biological ice nucleation
42 in clouds on a global scale?, Environmental Research Letters, 5, 024009, 10.1088/1748-
43 9326/5/2/024009, 2010.

- 1 Hoose, C., and Möhler, O.: Heterogeneous ice nucleation on atmospheric aerosols: a review
2 of results from laboratory experiments, *Atmospheric Chemistry and Physics*, 12, 9817-9854,
3 2012.
- 4 Huang, M., Xia, Z., Wang, H., Zeng, Q., and Wang, Q.: The range of the value for the
5 fuzzifier of the fuzzy c-means algorithm, *Pattern Recognition Letters*, 33, 2280-2284, 2012.
- 6 Huang, M., Hao, L., Guo, X., Hu, C., Gu, X., Zhao, W., Wang, Z., Fang, L., and Zhang, W.:
7 Characterization of secondary organic aerosol particles using aerosol laser time-of-flight mass
8 spectrometer coupled with FCM clustering algorithm, *Atmospheric Environment*, 64, 85-94,
9 2013.
- 10 Kamphus, M., Ettner-Mahl, M., Brands, M., Curtius, J., Drewnick, F., and Borrmann, S.:
11 Comparison of Two Aerodynamic Lenses as an Inlet for a Single Particle Laser Ablation
12 Mass Spectrometer, *Aerosol Science and Technology*, 42, 970-980, 2008.
- 13 Kamphus, M., Ettner-Mahl, M., Klimach, T., Drewnick, F., Keller, L., Cziczo, D. J., Mertes,
14 S., Borrmann, S., and Curtius, J.: Chemical composition of ambient aerosol, ice residues and
15 cloud droplet residues in mixed-phase clouds: single particle analysis during the Cloud and
16 Aerosol Characterization Experiment (CLACE 6), *Atmospheric Chemistry and Physics*, 10,
17 8077-8095, 2010.
- 18 Kandler, K., Lieke, K., Benker, N., Emmel, C., Küpper, M., Müller-Ebert, D., Ebert, M.,
19 Scheuvsens, D., Schladitz, A., Schütz, L., and Weinbruch, S.: Electron microscopy of particles
20 collected at Praia, Cape Verde, during the Saharan Mineral Dust Experiment: particle
21 chemistry, shape, mixing state and complex refractive index, *Tellus Series B - Chemical and
22 Physical Meteorology*, 63, 475-496, 2011.
- 23 Kaye, P. H., Hirst, E., Greenaway, R. S., Ulanowski, Z., Hesse, E., DeMott, P. J., Saunders,
24 C., and Connolly, P.: Classifying atmospheric ice crystals by spatial light scattering, *Optics
25 Letters*, 33, 1545-1547, 2008.
- 26 Klimach, T.: Chemische Zusammensetzung der Aerosole - Design und Datenauswertung
27 eines Einzelpartikel-Laserablationsmassenspektrometers, PhD thesis, University of Mainz,
28 Germany, 2012.
- 29 Koop, T., Luo, B. P., Tsias, A., and Peter, T.: Water activity as the determinant for
30 homogeneous ice nucleation in aqueous solutions, *Nature*, 406, 611-614, 2000.
- 31 Kupiszewski, P., Weingartner, E., Vochezer, P., Bigi, A., Rosati, B., Gysel, M., Schnaiter, M.,
32 and Baltensperger, U.: The Ice Selective Inlet: a novel technique for exclusive extraction of
33 pristine ice crystals in mixed-phase clouds, *Atmospheric Measurement Techniques
34 Discussions*, 7, 12481-12515, 2014.
- 35 Lance, S., Brock, C. A., Rogers, D., and Gordon, J. A.: Water droplet calibration of the Cloud
36 Droplet Probe (CDP) and in-flight performance in liquid, ice and mixed-phase clouds during
37 ARCPAC, *Atmospheric Measurement Techniques*, 3, 1683-1706, 2010.
- 38 Liu, P., Ziemann, P. J., Kittelson, D. B., and McMurry, P. H.: Generating Particle Beams of
39 Controlled Dimensions and Divergence: II. Experimental Evaluation of Particle Motion in
40 Aerodynamic Lenses and Nozzle Expansions, *Aerosol Science and Technology*, 22, 314-324,
41 1995a.
- 42 Liu, P., Ziemann, P. J., Kittelson, D. B., and McMurry, P. H.: Generating Particle Beams of
43 Controlled Dimensions and Divergence: I. Theory of Particle Motion in Aerodynamic Lenses
44 and Nozzle Expansions, *Aerosol Science and Technology*, 22, 293-313, 1995b.

1 Liu, P. S. K., Deng, R., Smith, K. A., Williams, L. R., Jayne, J. T., Canagaratna, M. R.,
2 Moore, K., Onasch, T. B., Worsnop, D. R., and Deshler, T.: Transmission Efficiency of an
3 Aerodynamic Focusing Lens System: Comparison of Model Calculations and Laboratory
4 Measurements for the Aerodyne Aerosol Mass Spectrometer, *Aerosol Science and*
5 *Technology*, 41, 721-733, 2007.

6 Lohmann, U., and Feichter, J.: Global indirect aerosol effects: a review, *Atmospheric*
7 *Chemistry and Physics*, 5, 715-737, 2005.

8 Mertes, S., Lehmann, K., Nowak, A., Massling, A., and Wiedensohler, A.: Link between
9 aerosol hygroscopic growth and droplet activation observed for hill-capped clouds at
10 connected flow conditions during FEBUKO, *Atmospheric Environment*, 39, 4247-4256,
11 2005.

12 Mertes, S., Verheggen, B., Walter, S., Connolly, P., Ebert, M., Schneider, J., Bower, K. N.,
13 Cozic, J., Weinbruch, S., Baltensperger, U., and Weingartner, E.: Counterflow Virtual
14 Impactor Based Collection of Small Ice Particles in Mixed-Phase Clouds for the Physico-
15 Chemical Characterization of Tropospheric Ice Nuclei: Sampler Description and First Case
16 Study, *Aerosol Science and Technology*, 41, 848-864, 2007.

17 Möhler, O., DeMott, P. J., Vali, G., and Levin, Z.: Microbiology and atmospheric processes:
18 the role of biological particles in cloud physics, *Biogeoscience*, 4, 1059-1071, 2007.

19 Möhler, O., Georgakopoulos, D. G., Morris, C. E., Benz, S., Ebert, V., Hunsmann, S.,
20 Saathoff, H., Schnaiter, M., and Wagner, R.: Heterogeneous ice nucleation activity of
21 bacteria: new laboratory experiments at simulated cloud conditions, *Biogeosciences* 5, 1425-
22 1435, 2008.

23 Murphy, D. M., Cziczo, D. J., Hudson, P. K., Thomson, D. S., Wilson, J. C., Kojima, T., and
24 Buseck, P. R.: Particle Generation and Resuspension in Aircraft Inlets when Flying in Clouds,
25 *Aerosol Science and Technology*, 38, 401-409, 2004.

26 Murphy, D. M., Hudson, P. K., Cziczo, D. J., Gallavardin, S., Froyd, K. D., Johnston, M. V.,
27 Middlebrook, A. M., Reinard, M. S., Thomson, D. S., Thornberry, T., and Wexler, A. S.:
28 Distribution of lead in single atmospheric particles, *Atmospheric Chemistry and Physics*, 7,
29 3195-3210, 2007.

30 Murray, B. J., Wilson, T. W., Dobbie, S., Cui, Z., Al-Jumur, S. M. R. K., Möhler, O.,
31 Schnaiter, M., Wagner, R., Benz, S., Niemand, M., Saathoff, H., Ebert, V., Wagner, S., and
32 Kärcher, B.: Heterogeneous nucleation of ice particles on glassy aerosols under cirrus
33 conditions, *Nature Geoscience*, 3, 233-237, 2010.

34 Murray, B. J., Broadley, S. L., Wilson, T. W., Atkinson, J. D., and Wills, R. H.:
35 Heterogeneous freezing of water droplets containing kaolinite particles, *Atmospheric*
36 *Chemistry and Physics*, 11, 4191-4207, 2011.

37 Murray, B. J., O'Sullivan, D., Atkinson, J. D., and Webb, M. E.: Ice nucleation by particles
38 immersed in supercooled cloud droplets, *Chemical Society reviews*, 41, 6519-6554, 2012.

39 Pratt, K. A., DeMott, P. J., French, J. R., Wang, Z., Westphal, D. L., Heymsfield, A. J.,
40 Twohy, C. H., Prenni, A. J., and Prather, K. A.: In situ detection of biological particles in
41 cloud ice-crystals, *Nature Geoscience*, 2, 398-401, 2009.

42 Pratt, K. A., Heymsfield, A. J., Twohy, C. H., Murphy, S. M., DeMott, P. J., Hudson, J. G.,
43 Subramanian, R., Wang, Z., Seinfeld, J. H., and Prather, K. A.: In Situ Chemical
44 Characterization of Aged Biomass-Burning Aerosols Impacting Cold Wave Clouds, *Journal*
45 *of the Atmospheric Sciences*, 67, 2451-2468, 2010.

- 1 Pratt, K. A., and Prather, K. A.: Aircraft measurements of vertical profiles of aerosol mixing
2 states, *Journal of Geophysical Research-Atmospheres*, 115, D11305, 2010.
- 3 Prenni, A. J., Petters, M. D., Kreidenweis, S. M., Heald, C. L., Martin, S. T., Artaxo, P.,
4 Garland, R. M., Wollny, A. G., and Pöschl, U.: Relative roles of biogenic emissions and
5 Saharan dust as ice nuclei in the Amazon basin, *Nature Geoscience*, 2, 402-405, 2009.
- 6 Pruppacher, H. R., and Klett, J. D.: *Microphysics of Clouds and Precipitation*, Kluwer
7 Academic Publishers, Dordrecht, 2010.
- 8 Rogers, D. C., DeMott, P. J., Kreidenweis, S. M., and Chen, Y. L.: Measurements of ice
9 nucleating aerosols during SUCCESS, *Geophysical Research Letters*, 25, 1383-1386, 1998.
- 10 Rolph, G. D.: Real-time Environmental Applications and Display sYstems (READY) Website
11 (<http://ready.arl.noaa.gov>), NOAA Air Resources Laboratory, Silver Spring, MD, 2014.
- 12 Rosati, B., Wehrle, G., Gysel, M., Zieger, P., Baltensperger, U., and Weingartner, E.: The
13 white-light humidified optical particle spectrometer (WHOPS) - a novel airborne system to
14 characterize aerosol hygroscopicity, *Atmospheric Measurement Techniques*, 8, 2015.
- 15 Roth, A.: Untersuchungen von Aerosolpartikeln und Wolkenresidualpartikeln mittels
16 Einzelpartikel-Massenspektrometrie und optischen Methoden, PhD thesis, University of
17 Mainz, Germany, 2014.
- 18 Schneider, J., Weimer, S., Drewnick, F., Borrmann, S., Helas, G., Gwaze, P., Schmid, O.,
19 Andreae, M. O., and Kirchner, U.: Mass spectrometric analysis and aerodynamic properties of
20 various types of combustion-related aerosol particles, *International Journal of Mass
21 Spectrometry*, 258, 37-49, 2006.
- 22 Seinfeld, J. H., and Pandis, S. N.: *Atmospheric Chemistry and Physics: From Air Pollution to
23 Climate Change*, John Wiley & Sons, Inc., New Jersey, 2006.
- 24 Slowik, J. G., Stainken, K., Davidovits, P., Williams, L. R., Jayne, J. T., Kolb, C. E.,
25 Worsnop, D. R., Rudich, Y., DeCarlo, P. F., and Jimenez, J. L.: Particle Morphology and
26 Density Characterization by Combined Mobility and Aerodynamic Diameter Measurements.
27 Part 2: Application to Combustion-Generated Soot Aerosols as a Function of Fuel
28 Equivalence Ratio, *Aerosol Science and Technology*, 38, 1206-1222, 2004.
- 29 Steinke, I., Hoose, C., Möhler, O., Connolly, P., and Leisner, T.: A new temperature- and
30 humidity-dependent surface site density approach for deposition ice nucleation, *Atmospheric
31 Chemistry and Physics* 15, 3703-3717, 2015.
- 32 Tenberken-Pötzsch, B., Schwikowski, M., and Gäggeler, H. W.: A method to sample and
33 separate ice crystals and supercooled cloud droplets in mixed phased clouds for subsequent
34 chemical analysis, *Atmospheric Environment*, 34, 3629-3633, 2000.
- 35 Tobo, Y., DeMott, P. J., Hill, T. C. J., Prenni, A. J., Swoboda-Colberg, N. G., Franc, G. D.,
36 and Kreidenweis, S. M.: Organic matter matters for ice nuclei of agricultural soil origin,
37 *Atmospheric Chemistry and Physics*, 14, 8521-8531, 2014.
- 38 Trimborn, A.: Online analysis of atmospheric particles with a transportable laser mass
39 spectrometer during LACE 98, *Journal of Geophysical Research*, 107, 8132, 2002.
- 40 Trimborn, A., Hinz, K.-P., and Spengler, B.: Online analysis of atmospheric particles with a
41 transportable laser mass spectrometer during LACE 98, *Journal of Geophysical Research*,
42 107, 8132, 2002.
- 43 Twohy, C. H., DeMott, P. J., Pratt, K. A., Subramanian, R., Kok, G. L., Murphy, S. M.,
44 Lersch, T., Heymsfield, A. J., Wang, Z., Prather, K. A., and Seinfeld, J. H.: Relationships of

1 Biomass-Burning Aerosols to Ice in Orographic Wave Clouds, *Journal of the Atmospheric*
2 *Sciences*, 67, 2437-2450, 2010.

3 Vali, G., DeMott, P. J., Möhler, O., and Whale, T. F.: Ice nucleation terminology,
4 *Atmospheric Chemistry and Physics Discussion*, 14, 22155-22162, 2014.

5 Vochezer, P., Järvinen, E., Wagner, R., Kupiszewski, P., Leisner, T., and Schnaiter, M.: In
6 situ characterization of mixed phase clouds using the Small Ice Detector and Particle Phase
7 Discriminator, submitted to *Atmospheric Measurement Techniques* 2015.

8 von Blohn, N., Mitra, S. K., Diehl, K., and Borrmann, S.: The ice nucleating ability of pollen:
9 Part III: New laboratory studies in immersion and contact freezing modes including more
10 pollen types, *Atmospheric Research*, 78, 182-189, 2005.

11 von der Weiden, S.-L., Drewnick, F., and Borrmann, S.: Particle Loss Calculator - a new
12 software tool for the assessment of the performance of aerosol inlet systems, *Atmospheric*
13 *Measurement Techniques*, 2, 479-494, 2009.

14 Weinbruch, S., Worringen, A., Ebert, M., Scheuven, D., Kandler, K., Pfeffer, U., and
15 Bruckmann, P.: A quantitative estimation of the exhaust, abrasion and resuspension
16 components of particulate traffic emissions using electron microscopy, *Atmospheric*
17 *Environment*, 99, 175-182, 2014.

18 Weingartner, E., Nyeki, S., and Baltensperger, U.: Seasonal and diurnal variation of aerosol
19 size distributions ($10 < D < 750$ nm) at a high-alpine site (Jungfrauoch 3580 m asl), *Journal of*
20 *Geophysical Research-Atmospheres*, 104, 26809-26820, 1999.

21 Wendisch, M.: A Quantitative Comparison of Ground-Based FSSP and PVM Measurements,
22 *Journal of Atmospheric and Oceanic Technology*, 15, 887-900, 1998.

23 Wise, M. E., Baustian, K. J., Koop, T., Freedman, M. A., Jensen, E. J., and Tolbert, M. A.:
24 Depositional ice nucleation onto crystalline hydrated NaCl particles: a new mechanism for ice
25 formation in the troposphere, *Atmospheric Chemistry and Physics*, 12, 1121-1134, 2012.

26 Worringen, A., Kandler, K., Benker, N., Dirsch, T., Mertes, S., Schenk, L., Kästner, U.,
27 Frank, F., Nillius, B., Bundke, U., Rose, D., Curtius, J., Kupiszewski, P., Weingartner, E.,
28 Vochezer, P., Schneider, J., Schmidt, S., Weinbruch, S., and Ebert, M.: Single-particle
29 characterization of ice-nucleating particles and ice particle residuals sampled by three
30 different techniques, *Atmospheric Chemistry and Physics*, 15, 4161-4178, 2015.

31 Zelenyuk, A., Cai, Y., and Imre, D.: From Agglomerates of Spheres to Irregularly Shaped
32 Particles: Determination of Dynamic Shape Factors from Measurements of Mobility and
33 Vacuum Aerodynamic Diameters, *Aerosol Science and Technology*, 40, 197-217, 2006.

34

1 Table 1: Cloud events during which measurements were taken behind Ice-CVI or ISI, along with the ALABAMA sampling time, the number of the
 2 measured spectra, the evaluation of the Ice-CVI-sampling-periods and the weather conditions and cloud formation during these events. The times of
 3 each cloud event based ^{a)} on the particle counter operated behind the Ice-CVI or ^{b)} on the liquid water content measured by two PVM instruments
 4 and a CDP outside the laboratory.

Event	Sampling time (local time)	Inlet	Number of spectra	Classification of the Ice CVI- sampling- periods	Weather conditions & clouds
1	^{a)} 22.01.2013 01:48 – 12:02	CVI	174	++	Warm front occlusive low pressure system; $\bar{T} = -19.2\text{ °C}$; wind direction $w_d = 325^\circ$; wind speed $\bar{v} = 8.1\text{ ms}^{-1}$
2	^{a)} 27.01.2013 16:27 – 28.01.2013 09:44	CVI	78	++	Occlusive frontal system, Ns; $\bar{T} = -12.7\text{ °C}$; $w_d = 318^\circ$; $\bar{v} = 8.4\text{ ms}^{-1}$
3	^{a)} 1. 29.01.2013 04:30 – 13:57 2. 29.01.2013 19:27 – 19:52	CVI	20 3	++ ++	Unstable warm front; first Ns than Cb; $\bar{T} = -7.8\text{ °C}$; $w_d = 320^\circ$; $\bar{v} = 12.6\text{ ms}^{-1}$
4	^{a)} 30.01.2013 16:14 – 31.01.2013 01:03	CVI	39	++	Squall line at cold front; Cb; $\bar{T} = -8.6\text{ °C}$; $w_d = 323^\circ$; $\bar{v} = 16.9\text{ ms}^{-1}$
5	^{a)} 1. 01.02.2013 17:22 – 02.02.2013 01:30 2. 02.02.2013 01:30 – 13:07 3. 02.02.2013 17:58 – 03.02.2013 01:00 4. 03.02.2013 01:00 – 10:45	CVI	134 701 209 73	++ + + ++	31.01.: cellular convection; Cu; $\bar{T} = -12.5\text{ °C}$; $w_d = 324^\circ$; $\bar{v} = 17.7\text{ ms}^{-1}$ 01.02. – 02.02.: frontal wave; Ns and Cb; $\bar{T} = -13.7\text{ °C}$; $w_d = 319^\circ$; $\bar{v} = 13.4\text{ ms}^{-1}$ Until 03.02. cellular convection; Cb; $\bar{T} = -23.1\text{ °C}$; $w_d = 308^\circ$; $\bar{v} = 9.7\text{ ms}^{-1}$

	b) 1. 31.01.2013 18:55 – 21:42 2. 01.02.2013 01:53 – 11:05	ISI	9 18		
6	a) 1. 05.02.2013 19:06 – 23:00 2. 05.02.2013 23:00 – 06.02.2013 04:20 3. 06.02.2013 04:20 – 05:00	CVI	24 42 3	++ + ++	Squall line at postfrontal convergence line; Cb; $\bar{T} = -19.8^{\circ}\text{C}$; wd = 331°; $\bar{v} = 10.5 \text{ ms}^{-1}$
7	a) 1. 06.02.2013 08:33 – 11:00 2. 06.02.2013 11:00 – 12:30 3. 06.02.2013 12:30 – 14:56 4. 06.02.2013 15:44 – 15:53 5. 06.02.2013 23:32 – 07.02.2013 04:30 6. 07.02.2013 04:30 – 08:45 7. 07.02.2013 08:45 – 09:49 8. 07.02.2013 20:29 – 08.02.2013 05:50 9. 08.02.2013 05:50 – 09:20	CVI	26 4 15 3 8 6 2 31 2	+ ++ + + ++ + ++ + ++	06.02: Convective dominating low-pressure vortex; Cb; $\bar{T} = -24.3^{\circ}\text{C}$; wd = 310°; $\bar{v} = 8.0 \text{ ms}^{-1}$ From 07.02. on: cellular convection; Cu; $\bar{T} = -20.8^{\circ}\text{C}$; wd = 324°; $\bar{v} = 7.6 \text{ ms}^{-1}$
8	a) 1. 09.02.2013 01:09 – 02:30 2. 09.02.2013 02:30 – 09:00 3. 09.02.2013 09:00 – 09:41	CVI	4 32 3	++ + ++	Diamond dust and cellular convection at convergence line; Ci, Cu (Cb); $\bar{T} = -26.7^{\circ}\text{C}$; wd = 316°; $\bar{v} = 7.2 \text{ ms}^{-1}$
9	a) 10.02.2013 18:10 – 18:24	CVI	2	++	Approaching warm front; Ci, Cs, As; $\bar{T} = -15.7^{\circ}\text{C}$; wd = 324°; $\bar{v} = 9.5 \text{ ms}^{-1}$
10	a) 1. 11.02.2013 08:03 – 10:31 2. 11.02.2013 15:08 – 12.02.2013 06:11	CVI	1 11	++ ++	Warm front; Ns; $\bar{T} = -18.7^{\circ}\text{C}$; wd = 227°; $\bar{v} = 6.6 \text{ ms}^{-1}$

11	^{a)} 12.02.2013 16:07 – 13.02.2013 01:33	CVI	8	++	Back of a low with northeast stream; Ns, Ac, As; $\bar{T} = -20.1^{\circ}\text{C}$; wd = 319°; $\bar{v} = 7.9 \text{ ms}^{-1}$
12	^{b)} 15.02.2013 01:17 – 09:10	ISI	114		Low pressure system; As, Cu, Cb, Ac; $\bar{T} = -16.9^{\circ}\text{C}$; wd = 322°; $\bar{v} = 7.7 \text{ ms}^{-1}$
13	^{a)} 19.02.2013 16:46 – 20.02.2013 16:47	CVI	1	++	Cold front from North; Ac, Ns, Sc, Cu; $\bar{T} = -14.3^{\circ}\text{C}$; wd = 321°; $\bar{v} = 8.2 \text{ ms}^{-1}$
14	^{b)} 24.02.2013 06:57 – 24.02.2013 09:31	ISI	3		Approaching warm front with precipitation; Cs, As, Ns; $\bar{T} = -20.4^{\circ}\text{C}$, wd = 150°; $\bar{v} = 8.5 \text{ ms}^{-1}$

1

2 Ac: altocumulus

3 As: altostratus

4 Cb: cumulonimbus

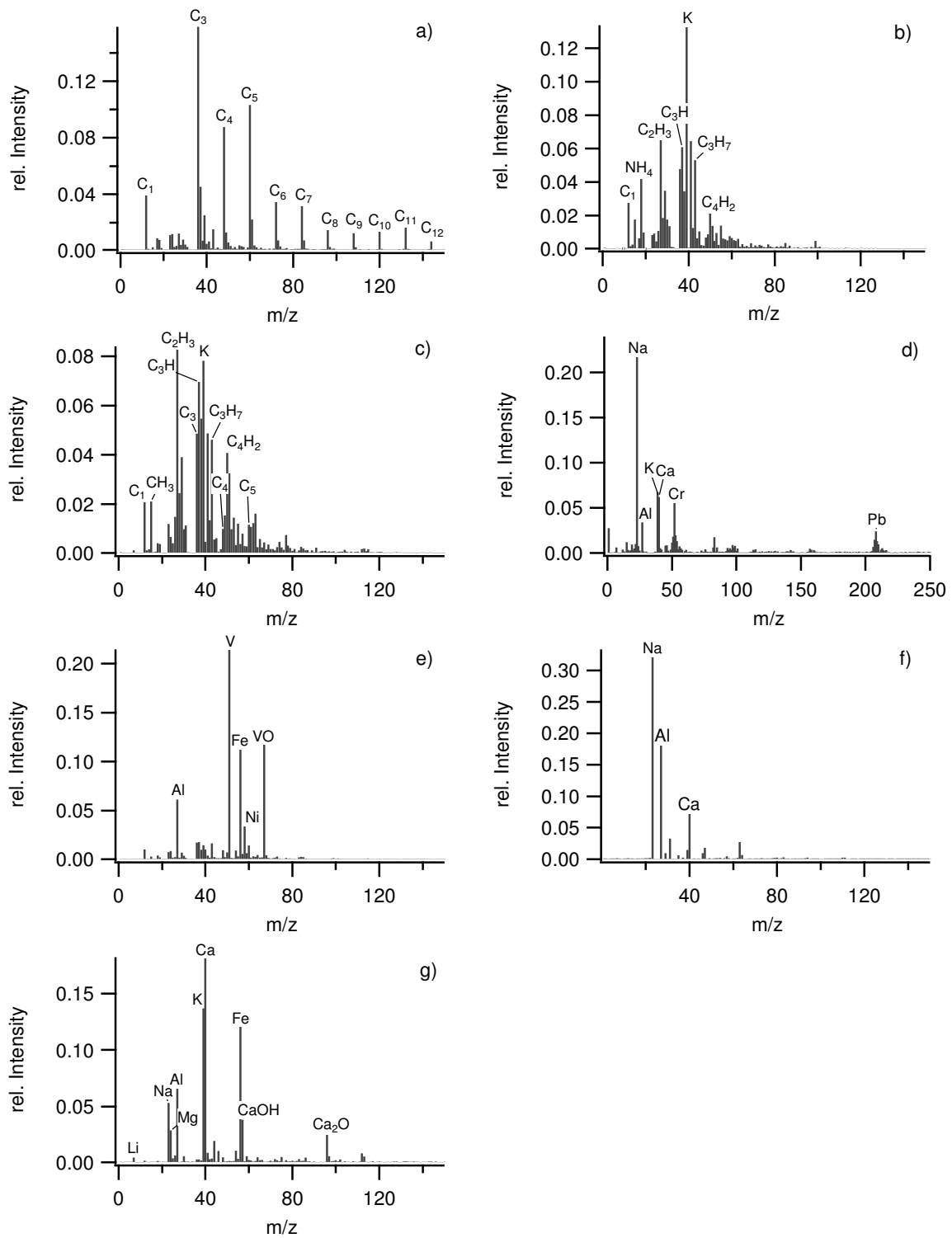
5 Ci: cirrus

6 Cs: cirrostratus

7 Cu: cumulus

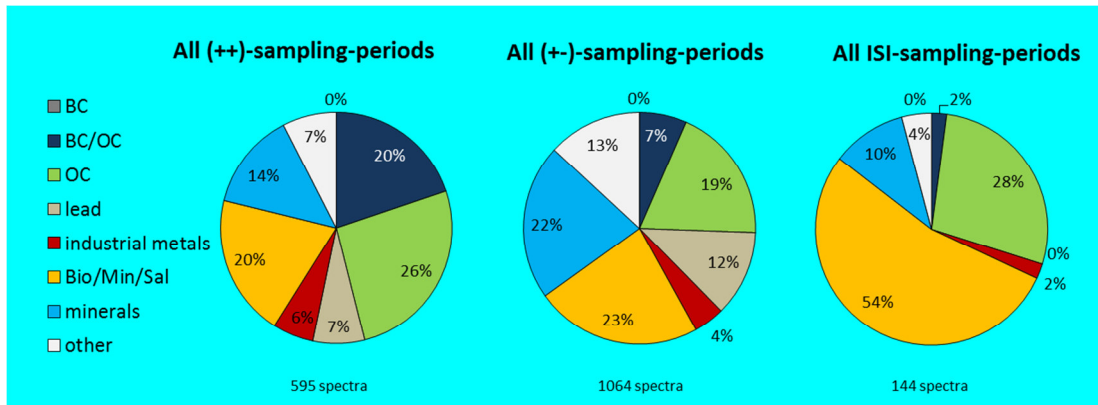
8 Ns: nimbostratus

9 Sc: stratocumulus



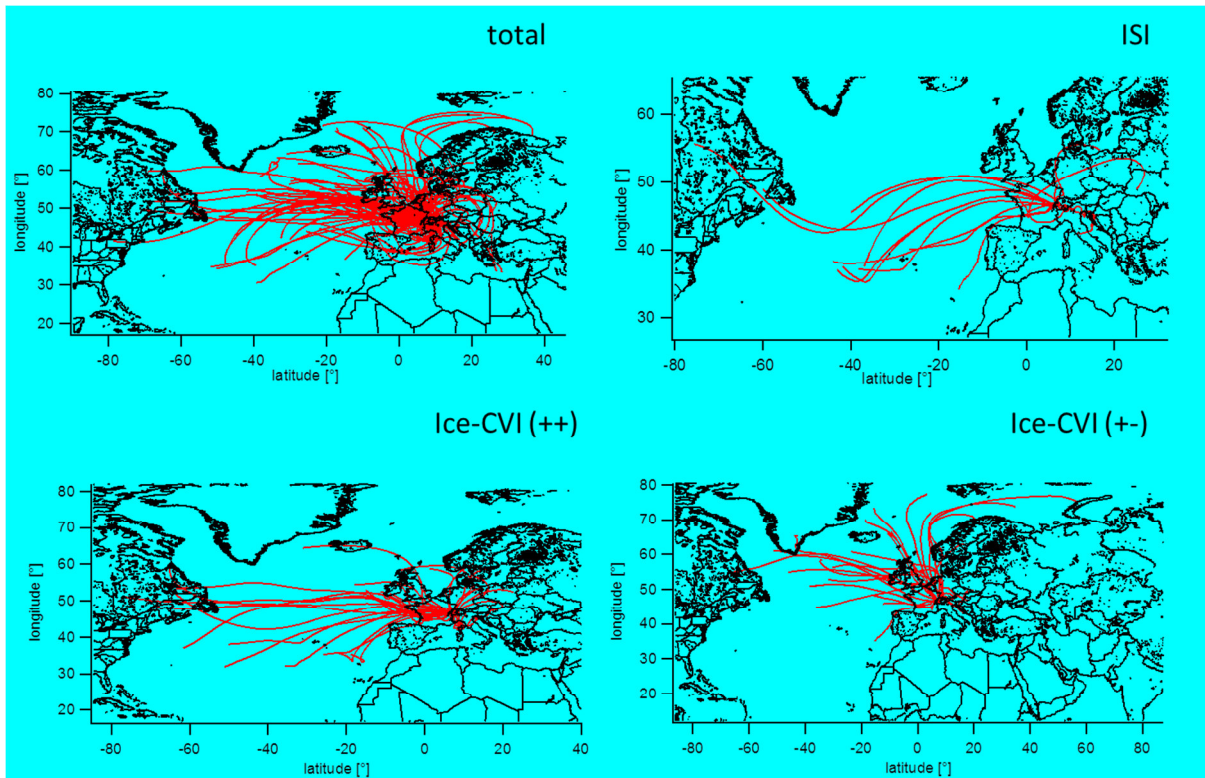
1
2
3
4
5
6

Figure 1: Average mass spectra of each particle type. a) black carbon; b) organic carbon; c) black carbon internally mixed with organic carbon; d) lead containing particles; e) industrial metals; f) **Bio/Min/Sal**; g) minerals



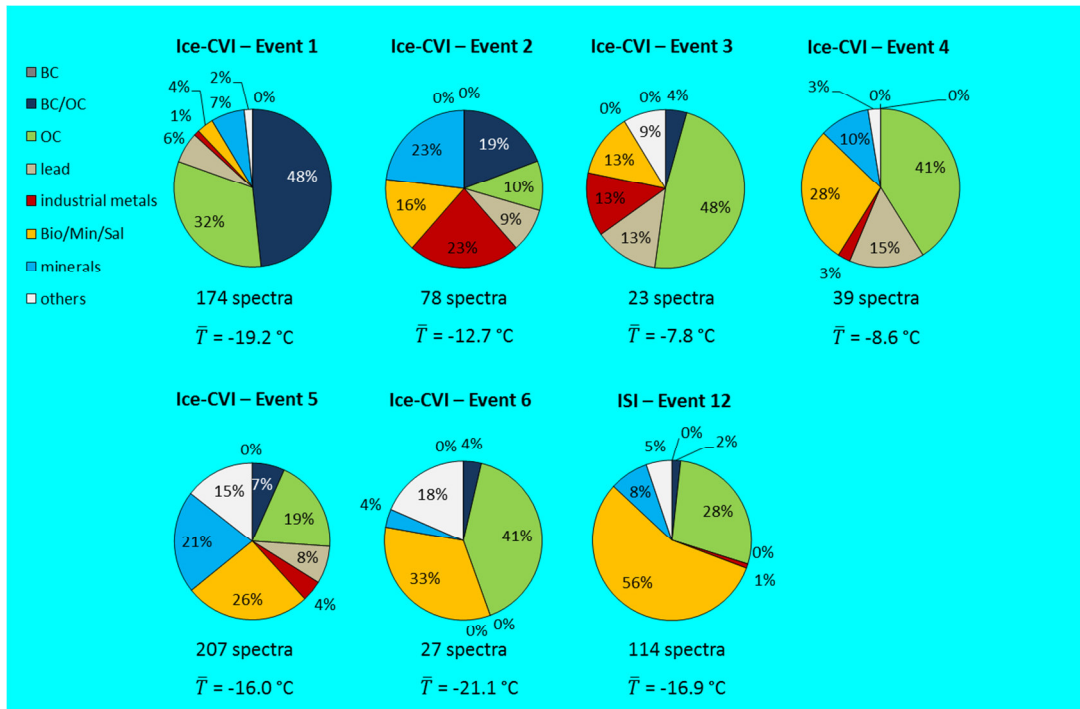
1
2
3
4
5
6

Figure 2: Results of the IPR composition analysis. Left and middle: measurements behind the Ice-CVI (left: all (++)-sampling-periods; middle: all (+-)-sampling-periods). Right: IPR composition measured behind the ISI.



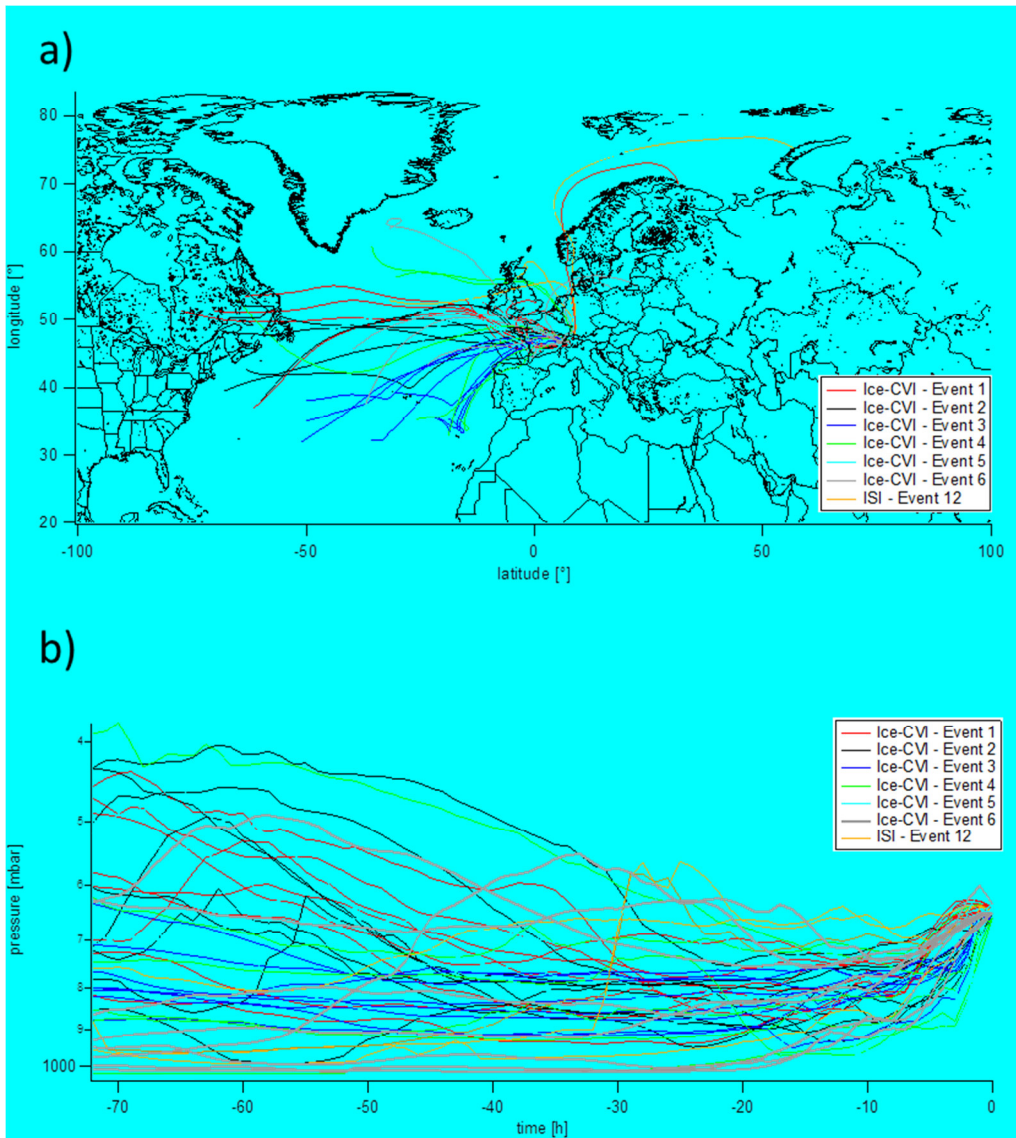
1
2
3
4
5
6

Figure 3: 72 h backward trajectories calculated with CRISP/HYSPLIT (one trajectory every 6 h)



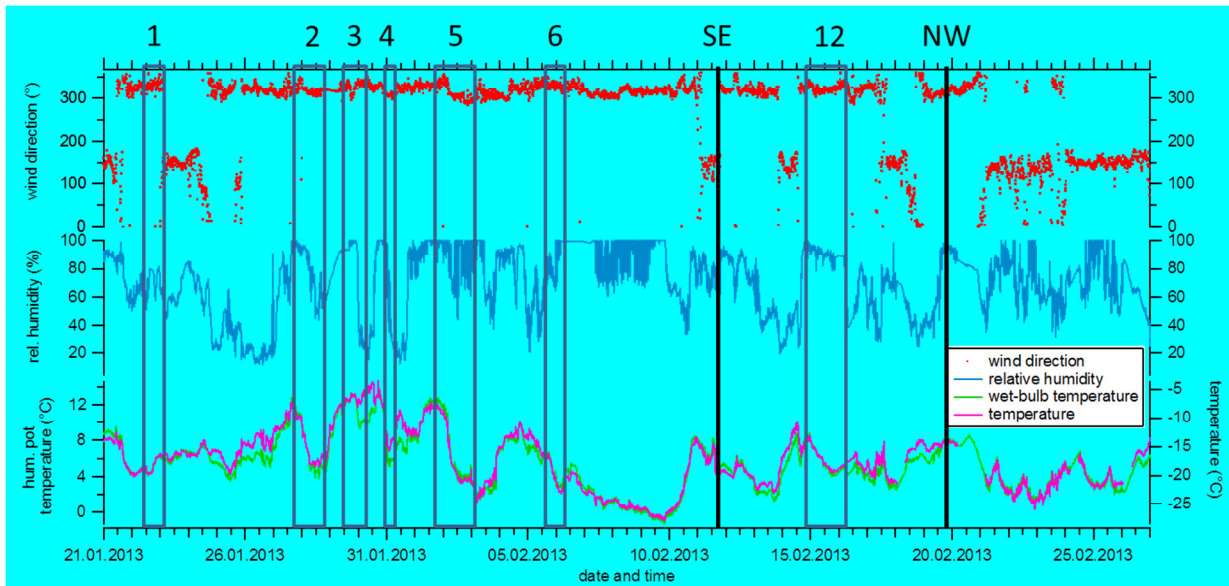
1
2
3
4
5
6
7
8
9
10

Figure 4: Comparison of the composition analysis of seven events measuring behind the Ice-CVI (all (++)-sampling-periods, Event 1: 22.01.2013 01:48 – 12:02; Event 2: 27.01.2013 16:27 – 28.01.2013 09:44; Event 3: 3.1 29.01.2013 04:30 – 13:57; 3.2 29.01.2013 19:27 – 19:52; Event 4: 30.01.2013 16:14 – 31.01.2013 01:03; Event 5: 5.1 01.02.2013 17:22 – 02.02.2013 01:30; 5.4 03.02.2013 01:00 – 10:45 and Event 6: 6.1 05.02.2013 19:06 – 23:00; 6.3 06.02.2013 04:20 – 05:00) and the ISI (Event 12: 15.02.2013 01:17 – 09:10) together with the corresponding average temperature during each event.



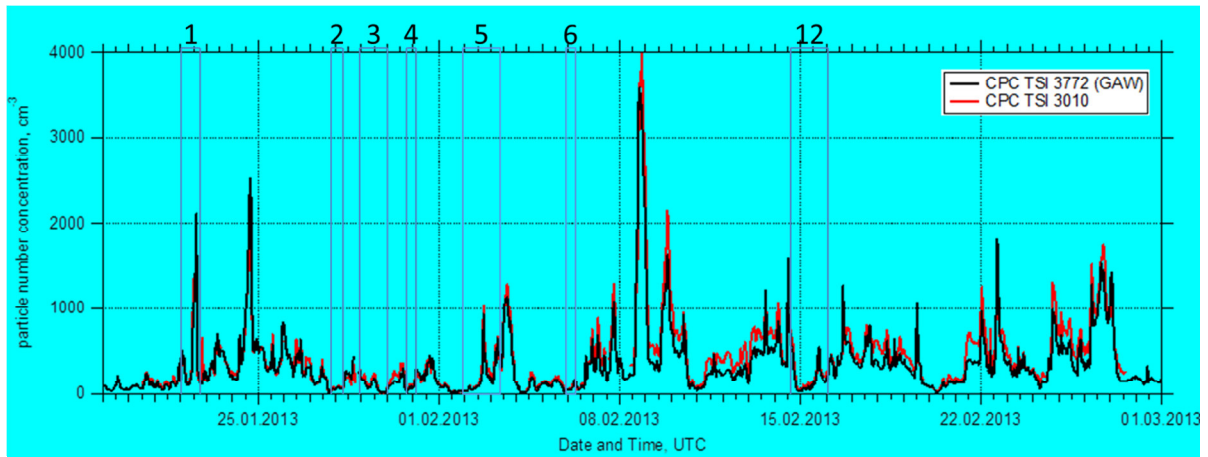
1
2
3
4
5
6

Figure 5: a) 72 h backward trajectories (one trajectory every three hours) calculated with CRISP for each event. b) The altitudes of air masses reaching the Jungfraujoeh as a function of time, converted to pressure units.



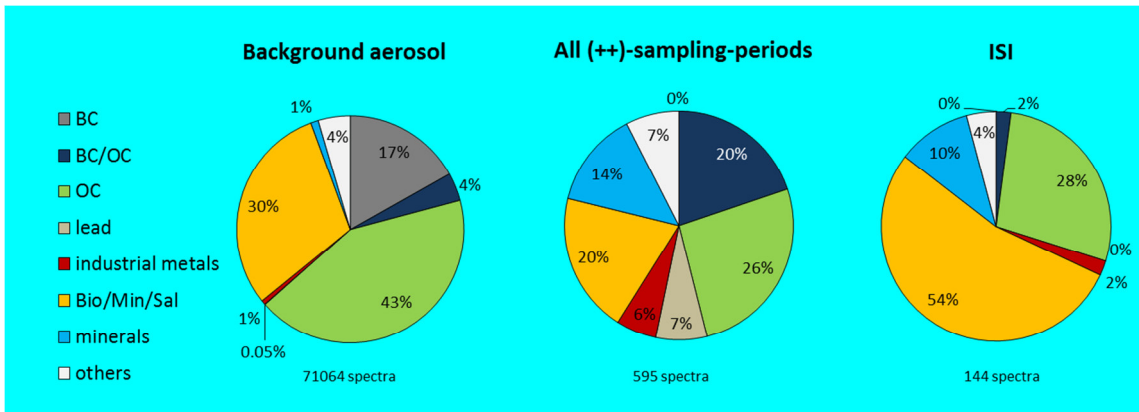
1
2

3 Figure 6: Wind direction, relative humidity, potential wet-bulb temperature and temperature
 4 over the whole measurement period (data from MeteoSwiss at the JFJ station). Black lines
 5 denote the events with different air mass origin (discussed in section 3.4). Events highlighted
 6 with blue bars denote the 7 different events from Section 2.1.1.



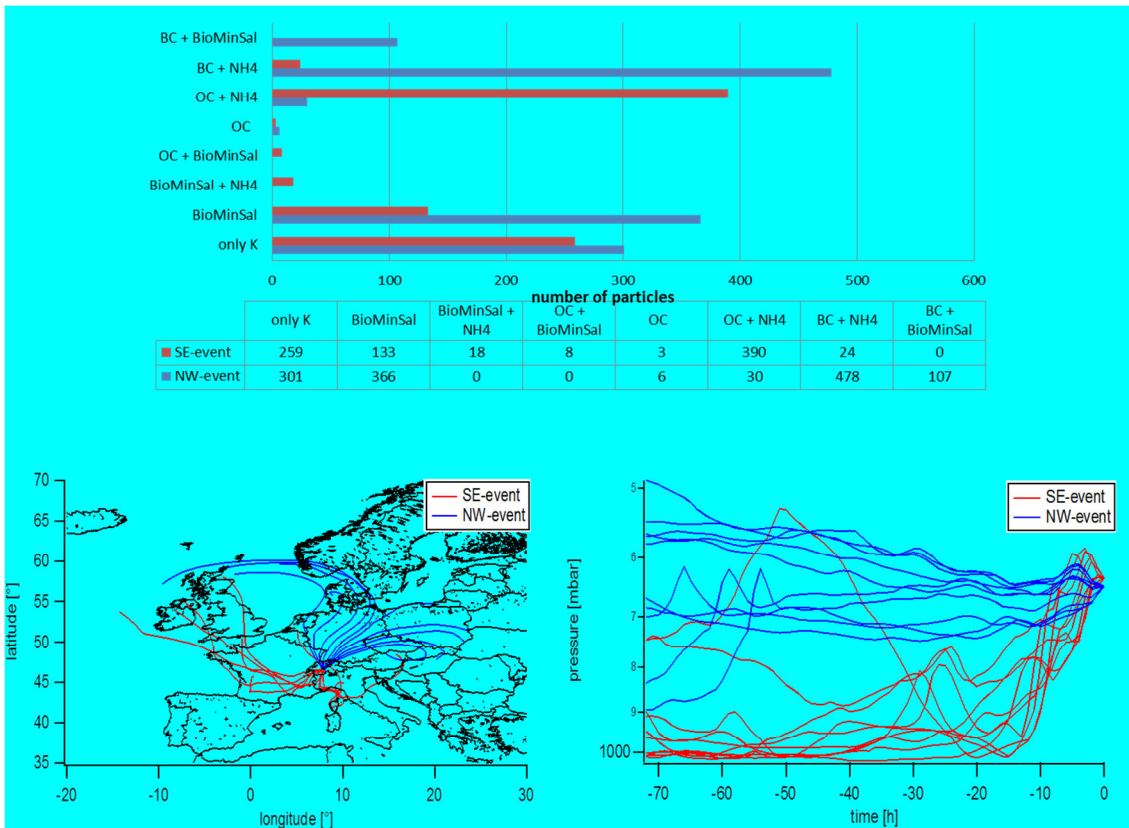
1
2
3
4
5
6
7
8
9

Figure 7: Particle number concentrations measured during the INUIT-JFJ/CLACE 2013 campaign by two different condensation particle counters (CPC): The GAW-CPC which is located directly behind the total inlet, and a TSI 3010 that was operated with a much longer sampling line (approx. 7 m) next to one of the aerosol mass spectrometers. Short elevated concentrations indicate local emissions. Events highlighted with blue bars denote the 7 different events from Section 2.1.1



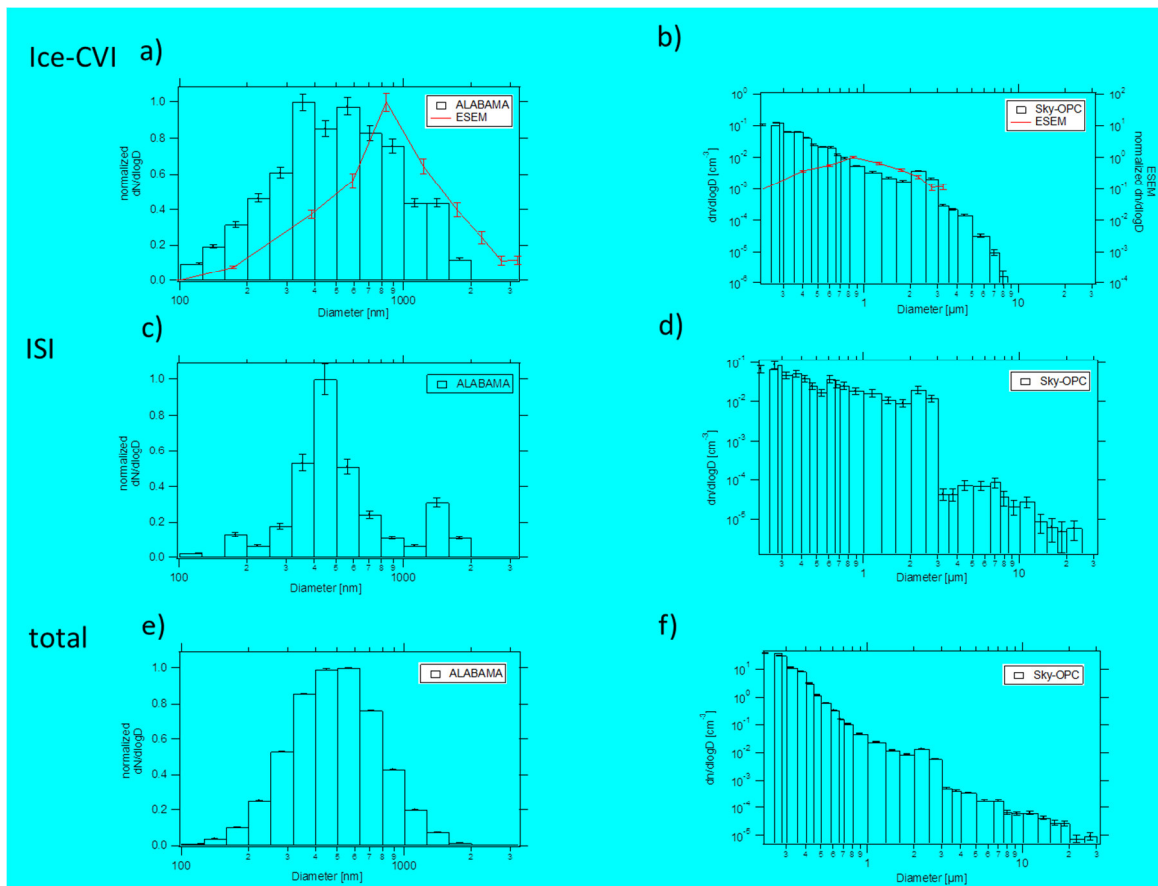
1
2
3
4
5

Figure 8: Comparison between the chemical composition of background aerosol particles (left) and IPR measured behind Ice-CVI (middle) and ISI (right).



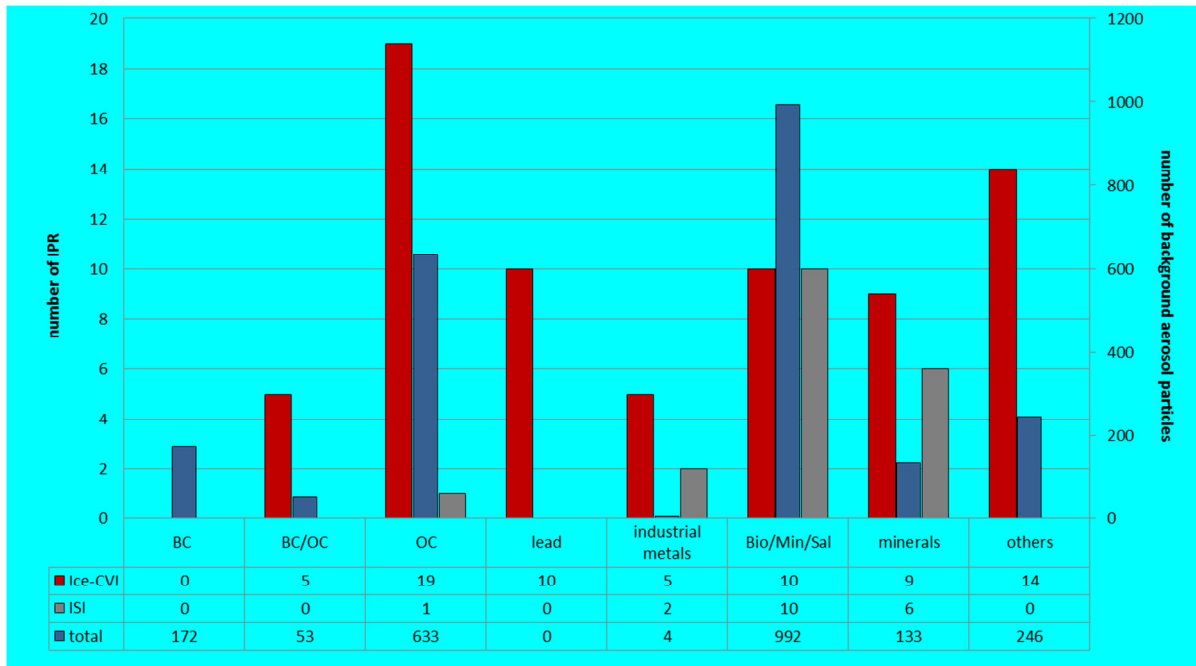
1
2
3
4
5
6
7
8

Figure 9: Comparison of two events measured during non-cloud episodes. The northwestern event (NW; blue) was on 19.02.2013 14:00 – 16:14 and the southeastern event (SE; red) was on 11.02.2013 10:32 – 14:27. 72 h back trajectories were calculated with one trajectory every 2 hours.



1
2
3
4
5
6
7
8
9
10
11
12
13

Figure 10: Measured size distribution of the IPR and background aerosol particles with the ALABAMA (bars; a, c, e) and Sky-OPC (bars; b, d, f) compared with the off-line SEM analysis of IPR samples (line; a and b). The error bars for the ALABAMA data result from counting statistics (averaged errors; $\Delta_{\text{Ice-CVI}} = 5.5\%$; $\Delta_{\text{ISI}} = 8.3\%$; $\Delta_{\text{total}} = 4\%$). The error of the OPC data results from Gaussian propagation of uncertainty, including counting statistics, the manufacturer-given error of the OPC of 3%, and the error of the enrichment factor (4% for the Ice-CVI and 20% for the ISI). The error of the ESEM dataset was determined by counting statistics. Note the different axis scaling. The y-axis is linear in a), c), e) and logarithmic in b), d), f). The x-axis range is 100 nm – 3250 nm in a), c), e) and 200 nm – 30 μm in b), d), f).



1
2
3
4
5
6

Figure 11: Chemical composition of IPR and background aerosol particles larger than 1000 nm measured behind the Ice-CVI (red), ISI (grey) and total inlet (blue). The error bars results from counting statistics.